

NEUROSYSTEMS

Modulation of the amplitude of γ -band activity by stimulus phase enhances signal encoding

Thomas Hoch,^{1,2} Stanislav Volgushev,³ Aleksey Malyshev,^{4,5,6} Klaus Obermayer^{1,2} and Maxim Volgushev^{4,5,6}

¹Neural Information Processing Group, Berlin University of Technology, Germany

²Bernstein Center for Computational Neuroscience, Berlin University of Technology, Germany

³Faculty for Mathematics, Ruhr University Bochum, Germany

⁴Department of Neurophysiology, Ruhr University Bochum, Germany

⁵Institute of Higher Nervous Activity and Neurophysiology, Russian Academy of Sciences, Moscow, Russia

⁶Department of Psychology, University of Connecticut, Storrs, CT 06269, USA

Keywords: cat, gamma oscillations, intracellular recordings, model, response selectivity, visual cortex

Abstract

Visual stimulation often leads to elevated fluctuations of the membrane potential in the γ -frequency range (25–70 Hz) in visual cortex neurons. Recently, we have found that the strength of γ -band fluctuations is coupled to the oscillation of the membrane potential at the temporal frequency of the stimulus, so that the γ -band fluctuations are stronger at depolarization peaks, but weaker at troughs of the stimulus frequency oscillation of the membrane potential. We hypothesized that this coupling may improve stimulus encoding. Here, we tested this hypothesis by using a single-compartment conductance-based neuron model, with parameters of the input adjusted to reproduce typical features of membrane potential and spike responses, recorded in cat visual cortical neurons *in vivo* during the presentation of moving gratings. We show that modulation of the γ -range membrane potential fluctuations by the amplitude of the slow membrane depolarization greatly improves stimulus encoding. Moreover, changing the degree of modulation of the γ -activity by the low-frequency signal within the range typically observed in visual cortex cells had a stronger effect on both the firing rates and information rates than changing the amplitude of the low-frequency stimulus itself. Thus, modulation of the γ -activity represents an efficient mechanism for regulation of neuronal firing and encoding of the temporal characteristics of visual stimuli.

Introduction

In the visual cortex, visual stimuli often evoke increases in activity in the high-frequency range, including the γ -band (25–70 Hz). The γ -range fluctuations may play an important role in cortical information processing. For example, synchronization of γ -activity across neurons that encode different features of an object may serve as a mechanism enabling feature-specific binding of neuronal responses (Eckhorn *et al.*, 1988; Gray & Singer, 1989; Singer, 1993, 1999; Jensen *et al.*, 2007; Lakatos *et al.*, 2008; Cardin *et al.*, 2009; Fries, 2009). Intracellular studies have revealed a number of properties of the γ -band fluctuations that enable them to subserve synchronization and patterning of neuronal activity, for example the abilities to support reliable spike generation, impose precise temporal windows for synaptic integration, and produce precise temporal patterns of activity (Lampl & Yarom, 1993; Mainen & Sejnowski, 1995; Nowak *et al.*, 1997; Volgushev *et al.*, 1998, 2003; Salinas & Sejnowski, 2000; Fries *et al.*, 2007). γ -Band fluctuations originate from the precise temporal organization of excitatory and inhibitory inputs, with possible additional contributions of intrinsic membrane mechanisms of some

cells (Jagadeesh *et al.*, 1992; Jahnsen & Karnup, 1994; Gutfreund *et al.*, 1995; Gray & McCormick, 1996; Hutcheon *et al.*, 1996; Binguier *et al.*, 1997; Lampl *et al.*, 1999; Azouz & Gray, 1999, 2003, 2008; Cunningham *et al.*, 2004; Hasenstaub *et al.*, 2005; Bartos *et al.*, 2007; Sohal *et al.*, 2009). The power of high-frequency fluctuations depends on stimulus orientation, correlating with spike responses (Jagadeesh *et al.*, 1992; Azouz & Gray, 1999; Volgushev *et al.*, 2003), but also changes spontaneously on a trial-to-trial basis (Azouz & Gray, 1999, 2003) or with alternation of active and silent states in neocortical neurons during slow oscillation (Steriade *et al.*, 1996; Anderson *et al.*, 2000b; Mukovski *et al.*, 2006).

Simple cells in the visual cortex encode temporal characteristics of visual stimuli in their firing (Dean & Tolhurst, 1983; Skottun *et al.*, 1991), which is coupled to depolarizations of the membrane potential at the stimulation frequency (Carandini & Ferster, 2000; Volgushev *et al.*, 2003; Azouz & Gray, 2008). Because, in visual cortex neurons, the amplitude of the γ -band fluctuations correlates with the amplitude of the low-frequency, stimulus-induced membrane potential changes, we have hypothesized that this coupling may improve stimulus encoding (Volgushev *et al.*, 2003). Here, we exploited a combination of electrophysiological and computational approaches to test this hypothesis. Using *in vivo* intracellular recordings from cat visual cortex neurons, we have characterized their membrane potential and

Correspondence: Maxim Volgushev, ⁶Department of Psychology, as above.
E-mail: maxim.volgushev@uconn.edu

Received 22 October 2010, accepted 15 December 2010

spike responses to the presentation of moving sinusoidal gratings and information rate in the spike responses. For computational analysis, we have constructed a Hodgkin–Huxley-type model and tuned the input conductances to reproduce in the model neuron the responses with characteristics measured *in vivo*. Using this model, we studied how the low-frequency and high-frequency components of membrane potential responses contribute to the information rate in neurons' firing, and tested our hypothesis that coupling of the γ -power to the amplitude of low-frequency membrane potential fluctuations improves stimulus encoding.

Materials and methods

Physiology

Experiments were performed on adult cats (3–4.5 kg). The procedures were in accordance with the guidelines published in the European Communities Council Directive (86/609/EEC, 1986) and were approved by a local animal welfare committee (Bezirksregierung Ansberg, Germany). Surgery and maintenance of animals were similar to those described in detail previously (Volgushev *et al.*, 2000, 2003). The experimental data reported here were obtained from five adult cats. Cats were anesthetized with ketamine hydrochloride (Ketanest; Parke-Davis GmbH, Germany; 0.3 mL/kg) and Rompun (Bayer, Germany; 0.08 mL/kg). During the experiment, adequate anesthesia was maintained with a gas mixture of N₂O/O₂ (70 : 30) and 0.2–0.4% halothane (Eurim-Pharm, Germany). Surgery was started after stable anesthesia with complete analgesia was achieved. The animal was placed in a stereotaxic frame, the skull was exposed, and a craniotomy was performed over area 17 of the visual cortex. Fluid replacement was achieved by the intra-arterial administration of 6 mL/h of Ringer solution containing 1.25% glucose. Neuromuscular blockade was induced by intra-arterial infusion of alcuronium chloride (0.15 mg/kg/h) in Ringer solution. Artificial respiration was performed with a cat/rabbit ventilator (Model 6025; Ugo Basile, Biological Research Apparatus, Comariva-Varese, Italy). The volume (20–40 cm³) and the rate of stroke (7–15/min) were adjusted to maintain end-tidal CO₂ between 3.5 and 4.0%. End-tidal CO₂, body temperature, heart rate, blood pressure and electroencephalogram were continuously monitored. At the end of the experiment, animals were killed by increasing the halothane concentration and injection of an overdose of barbiturate. Intracellular recordings were made with sharp electrodes, filled with 2.5 M potassium acetate. The electrode resistance was 70–120 M Ω . Neurons with a stable resting membrane potential were recorded for at least 15 min at a sampling frequency of 10–40 kHz. Visual responses were evoked by moving sinusoidal gratings with optimal temporal frequency (0.5–2.5 Hz for different neurons) and different orientations, which were presented on a screen in front of the animal. Gratings of different orientations were presented in pseudo-random order. The gratings were generated with subroutines of the VISION WORKS stimulation system (Cambridge Research Systems, NH, USA) and our own programs.

Single-compartment model

For all simulations in this study, we used a single-compartment conductance-based model adapted from Wang & Buzsaki (1996) and modified as described below. The model contained Hodgkin–Huxley-type ion currents and time-dependent excitatory and inhibitory synaptic conductances. Changes in the membrane potential V of the model neuron are described by the following differential equation:

$$C_m \frac{dV}{dt} = -I_L - I_{Na} - I_K - I_M - I_{syn}, \quad (1)$$

where $C_m = 1 \mu\text{F}/\text{cm}^2$ is the membrane capacitance, I_L is the leak current, I_{Na} and I_K are the voltage-gated sodium and potassium currents mediating spike generation, I_M is a non-inactivating potassium current for spike frequency adaptation, and I_{syn} is the total synaptic current. The dynamics of each ionic current (for synaptic see below) are given by the following equation:

$$I(t) = g(t)[V(t) - E_{\text{reversal}}], \quad (2)$$

where $g(t)$ is the respective ionic conductance, and E_{reversal} is reversal potential of that current. For the leak current, the reversal potential was $E_L = -75$ mV, and the leak conductance $g_L = 0.05$ mS/cm² did not change with time, but remained constant. As this model was originally developed to simulate a network of fast-spiking interneurons, we have adjusted it as follows. To account for the fast initiation dynamics of action potentials in neocortical neurons (Naundorf *et al.*, 2006), we set the kinetics of sodium channels to be 10 times faster, and the width of their activation curve to be two times narrower, than in the original model. This allowed to bring the firing patterns and rates during stimulation, as well as the shape of the generated action potentials, closer to the experimental data. Details of the kinetic equations of the intrinsic currents and the other model parameters are given in the Appendix.

The total synaptic current I_{syn} , which represents the synaptic input evoked by the visual stimulation as well as the background activity, is described as:

$$I_{syn}(t) = g_e(t)(V(t) - E_e) + g_i(t)(V(t) - E_i), \quad (3)$$

where $g_e(t)$ and $g_i(t)$ are stochastic processes that represent the conductance at the excitatory and inhibitory synapses, and E_e and E_i are reversal potentials of the excitatory and inhibitory currents. The excitatory and inhibitory fluctuating conductances were adjusted to reproduce in the model neuron fluctuations of the membrane potential with characteristics similar to those measured in cat neurons *in vivo* during presentation of moving gratings of optimal and non-optimal orientation. Responses of cat visual cortex neurons to moving gratings and details of the adjustment of the model parameters to the experimental data are explained in Results.

Processing of membrane potential traces

Membrane potential traces recorded in cat neurons *in vivo* and simulated with computer models were processed with the same procedures. Action potentials were detected by the threshold (usually 30–40 mV from the mean resting membrane potential), and their onset time was then determined as the point at which the rate of change of the membrane potential dV/dt first exceeded 5% of the maximal rate of dV/dt for the action potentials of that neuron. The resulting time sequences of action potentials were used for calculation of firing rates, spike responses to visual stimuli, and information rate (see below for details). For further analysis of membrane potential traces, spikes were removed with the procedure established in our previous work (Volgushev *et al.*, 2003). In brief, action potentials were removed from 0.7 ms before the onset to T_{post} after it, and the membrane potential between these two points was linearly interpolated. T_{post} (usually 3–5 ms) was adjusted individually for each cell to ensure complete removal of the entire action potential waveform, as verified by visual inspection of the voltage traces. For spectral analysis of the

membrane potential and extraction of its frequency components, the fast Fourier transform (FFT) was used. We opted for the FFT for several reasons. First, the FFT allows precise definition of frequency bands and extraction of respective components of a signal. Second, the FFT and inverse FFT allow bi-directional transformation of the signal between frequency domain and time domain. Combination of these features is important for tuning the neuron model to reproduce experimentally measured responses in simulations, for example relationships between low-frequency and high-frequency components of membrane potential fluctuations (see Results).

The stimulus-induced component and the γ -range component of the membrane potential fluctuations were extracted as follows. First, we transformed the membrane potential into Fourier space using the FFT function of MATLAB 6.5 (MathWorks, Natick, MA, USA), and then we set all coefficients corresponding to frequencies outside the desired range to zero and performed the inverse FFT to transform the result back to the time domain. For extraction of the low-frequency stimulus-induced component, the coefficients corresponding to the stimulation frequency ± 0.5 Hz were used; for example, for a 2-Hz moving grating, Fourier coefficients between 1.5 and 2.5 Hz were used while all other coefficients were set to zero. With the inverse FFT, the result was transformed back to the time domain (e.g. thick blue trace in Fig. 1B). The power of this component is referred to in the subsequent text as stimulus power. The γ -range component was extracted with the same procedures, that is, by setting all Fourier coefficients for frequencies outside of the γ -range (25–70 Hz) to zero. The power of this component is referred to in the subsequent text as γ -power. After transformation back to the time domain with inverse FFT, the γ -range component was used for representation purposes (e.g. Fig. 1C), and for calculating the relationship between the amplitude of the slow, stimulus-induced changes of the membrane potential and the amplitude of the γ -range fluctuations. This relationship was quantified as follows. First, we estimated the power of the γ -range fluctuations of the membrane potential, using a running rectangular window of 102.4-ms width and with a time step of 10 ms (e.g. Fig. 1B, red trace). We then calculated the linear correlation coefficient between the resulting signal and the low-frequency component. Note that the above procedure leads to a smoothed signal for the γ -power (because of the sliding overlapping window), leading to a linear correlation coefficient that is lower than 1 even for the case when the γ -range fluctuations are perfectly correlated with the low-frequency component of the membrane potential (for a further discussion, see Fig. 5 and related text). The running average of the γ -power provides a better formalized and more reliable measure for assessing its relationship with the slow changes of the membrane potential than the envelope-based measures used in our previous study (Volgushev *et al.*, 2003). These advantages are important for using the experimental results as constraints for the tuning of neuron models for simulations.

Estimation of the information rate

To assess how different components of membrane potential responses influence the encoding of stimulus in neurons' firing, we adopted an information theory approach, which provides the most rigorous way of assessing the quality of stimulus encoding. To estimate the information rate in our intracellular recordings and simulation experiments, we exploited a linear filter approach, which has been widely used in computational neuroscience studies (Bialek *et al.*, 1991; Gabbiani, 1996; Rieke *et al.*, 1997; for a review see Borst & Theunissen, 1999).

In this approach, a lower bound on the information rate between stimulus and response can be obtained with the following equation (Gabbiani, 1996; Borst & Theunissen, 1999):

$$I_{LB} = -\frac{1}{2\pi} \int_0^{\infty} \log_2[1 - \gamma^2(\omega)] d\omega. \quad (4)$$

where the function

$$\gamma^2(\omega) = \frac{|P_{SR}(\omega)|^2}{P_{SS}(\omega)P_{RR}(\omega)} \leq 1, \quad (5)$$

is the coherence between the stimulus and the response, ω denotes frequency, $P_{SS}(\omega)$ and $P_{RR}(\omega)$ are the power spectra of the stimulus and the spike train, and $P_{SR}(\omega)$ is their cross-spectrum. The coherence $\gamma^2(\omega)$ was calculated as follows. From the membrane potential traces of 5000-ms duration, which were recorded during grating movement, we extracted the low-frequency stimulus-induced component (temporal frequency of the stimulus, ± 0.5 Hz) of the membrane potential fluctuations. This component reflects periodic changes in input to the recorded neuron, which are produced by a sinusoidal grating moving over receptive fields of the input neurons. It was used to calculate the power spectrum of the stimulus and the cross-correlation between the stimulus and the spike train in Eqn (5). This approach allows use of the same processing of data obtained in experiments and in computer simulations. The spike response was constructed as a train of delta pulses occurring at spike onset times, determined as described above. To calculate power spectra, the respective signal (voltage trace or spike response) was divided into segments of 819.2-ms duration, with an overlap of 50%. Each segment was multiplied by a normalized Hann window function w , and the result, X^*w , was transformed into Fourier space. Then, $P_{XX} = \langle X(\omega)X(\omega)^* \rangle$ was calculated, where $X(\omega)$ is the Fourier transform of X^*w , $X(\omega)^*$ is the complex conjugate, and $\langle \rangle$ denotes the averaging over segments. The cross-spectrum (P_{XY}) was calculated as $P_{XY}(\omega) = \langle X(\omega)Y(\omega)^* \rangle$. The same procedure was used for the calculation of the information rate of the simulated traces, which had a duration of 200 s.

Results

The aim of this study was to test the hypothesis that coupling of the strength of the high-frequency fluctuations to the amplitude of the membrane potential oscillation at the temporal frequency of the stimulus may improve stimulus encoding (Volgushev *et al.*, 2003). To this end, we first describe intracellularly recorded responses of cat visual cortex neurons to the presentation of moving sinusoidal gratings *in vivo*. These *in vivo* data were used to obtain key characteristics of the membrane potential changes, spike responses, and stimulus encoding, which were then used as constraints for model tuning and as a reference for the comparison of simulation results. Next, we describe how input conductances, which reproduced in a model neuron the main parameters of the recorded membrane potential traces, were constructed. Finally, we studied in the model neuron how stimulus encoding is influenced by changes in the amplitude of the low-frequency component (stimulus, 2 Hz) and high-frequency component (γ -range, 25–70 Hz) of the input conductances and by the strength of their correlation.

Intracellular recordings from cat visual cortex neurons *in vivo*

Intracellular recordings were made from neurons in cat visual cortex *in vivo*. For the analysis, we selected nine neurons from a sample of 34 cells recorded in five cats. These nine neurons were selected for analysis because they were tested with moving sinusoidal gratings and showed clear response modulation at the temporal frequency of the optimally oriented moving grating, and thus had

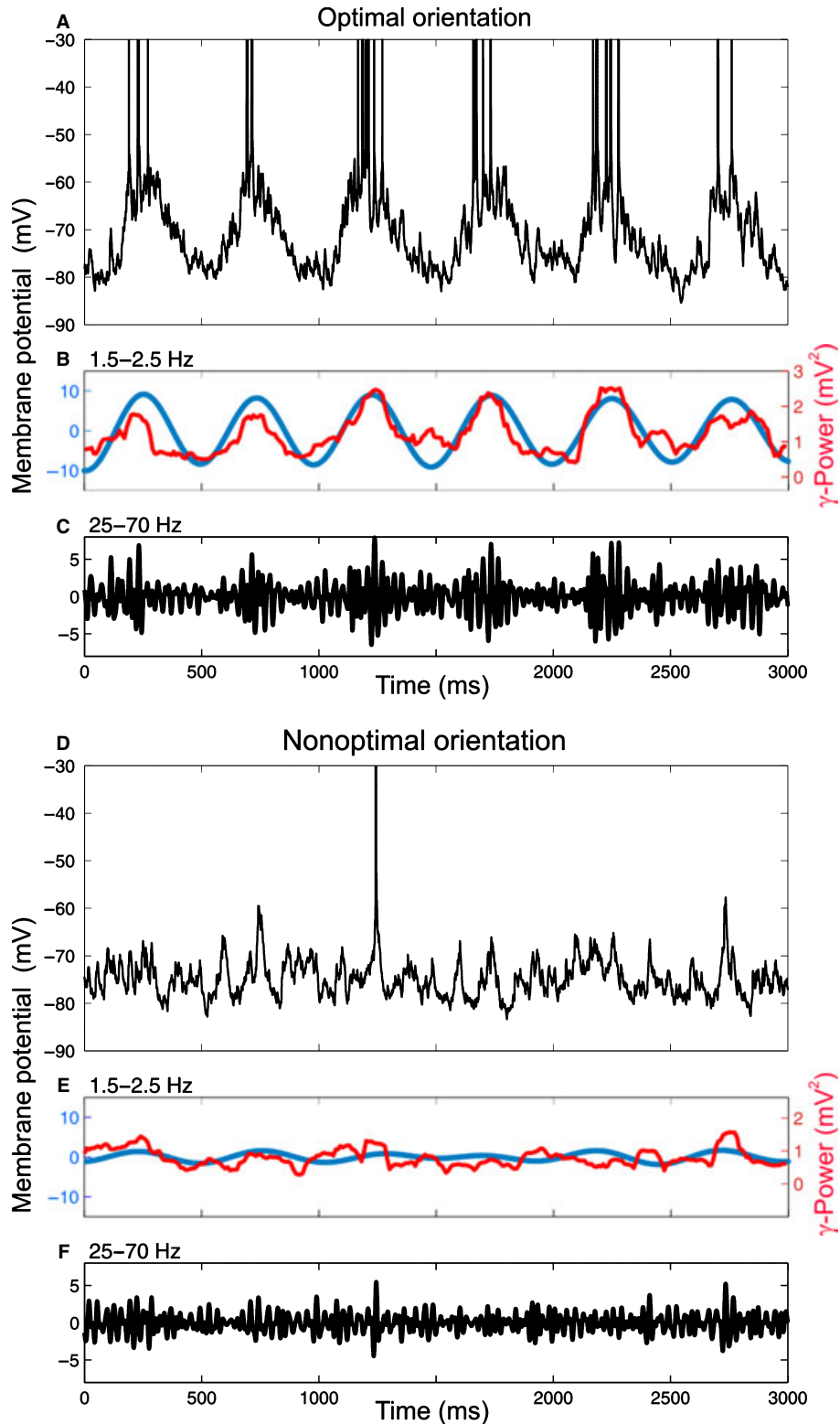


FIG. 1. Responses of a cell in cat visual cortex to moving sinusoidal gratings with optimal (A) and non-optimal (D) orientations and their analysis. (A and D) Membrane potential traces. The temporal frequency of the moving grating was 2 Hz. Action potentials are truncated. (B, C, E and F) Analysis of the relationship between the low-frequency component (1.5–2 Hz, blue/gray lines in B and E, scale on the left) and the high-frequency, γ -range component (25–70 Hz, C and F) from the traces in A and D. In B and E, red/black lines (scale on the right) show the power of the γ -range fluctuations calculated in a running window of 102.4 ms. Note that the γ -power curves are scaled to match the amplitude of the respective low-frequency components. For interpretation of references to color in the figure legend, please refer to the Web version of this article.

simple receptive fields (Dean & Tolhurst, 1983; Skottun *et al.*, 1991; Carandini & Ferster, 2000; Volgushev *et al.*, 2003). Seven of the nine cells were not used in previous studies; the remaining two cells were from the sample presented in Volgushev *et al.* (2003). In these recordings, we analyzed key features of the cellular responses to the presentation of moving gratings with different orientations and directions of movement. Specifically, we quantified the relationship between stimulus orientation/direction of movement, and low-frequency modulation of the membrane potential at the temporal frequency of stimulation (the optimal frequency for different neurons was 0.5–2.5 Hz), high-frequency (25–70 Hz) fluctuations of the membrane potential, and spike responses. We also characterized the relationship between low-frequency and high-frequency fluctuations of the membrane potential, and encoding of the stimulus in the spike trains of recorded neurons.

Figure 1 shows an example of membrane potential traces of a visual cortex cell during responses to the presentation of a moving grating with optimal (Fig. 1A) and non-optimal orientation (Fig. 1D). A moving grating with optimal orientation induced strong modulation of the membrane potential at the temporal frequency of stimulation (2 Hz for this neuron), accompanied by strong fluctuations in the high-frequency range and bursts of action potentials at depolarization peaks (Fig. 1A). The low-frequency (stimulus frequency, ± 0.5 Hz, thus 1.5–2.5 Hz) modulation reached about 20-mV peak-to-peak amplitude (Fig. 1B, blue/gray trace). High-frequency components (25–70 Hz; γ -range) of the membrane potential fluctuations were estimated after spike removal (see Materials and methods for details). High-frequency fluctuations of the membrane potential reached a peak-to-peak amplitude of more than 10 mV (Fig. 1C). Comparison of the two components demonstrates clearly that the strength of the γ -range fluctuations correlated with the amplitude of the slow membrane potential modulation at the stimulus frequency. The amplitude of high-frequency fluctuations was high at depolarizing peaks (positive phase) of the stimulus frequency modulation, but much lower during negative phases, at relatively hyperpolarized membrane potentials. To quantify the relationship between the modulation of the membrane potential at the stimulus frequency (blue/gray trace in Fig. 1B) and the power of the γ -range fluctuations, we first calculated a running average of the γ -power (red/black trace in Fig. 1B; see Materials and methods for details), and then calculated the linear correlation coefficient between these two signals. The γ -power was significantly correlated with the slow modulation of the membrane potential at stimulus frequency ($r = 0.67$).

During presentation of an orthogonally oriented (non-optimal) grating, both the low-frequency modulation and high-frequency fluctuations of the membrane potential were much weaker, and action potentials were generated only occasionally (Fig. 1D). Because of the lower regularity and the low amplitude of the membrane potential changes, a comparison of the low-frequency (Fig. 1E) and high-frequency (Fig. 1F) components does not reveal a clear relationship. The correlation between the power of γ -range fluctuations and the amplitude of slow membrane depolarizations was weaker, but still significant ($r = 0.40$, $P < 0.01$).

To compare the spectral compositions of membrane potential traces during the presentation of optimal and non-optimal stimuli, we calculated their power spectra. The power spectra in Fig. 2A (thick green/gray curve for optimal orientation, and thin red/black curve for non-optimal orientation) and their ratio (Fig. 2B; the horizontal line is ratio = 1) show that the most pronounced difference between the responses to the optimal and non-optimal orientation occurred in two frequency ranges. First, optimal stimuli evoked much stronger modulation of the membrane potential

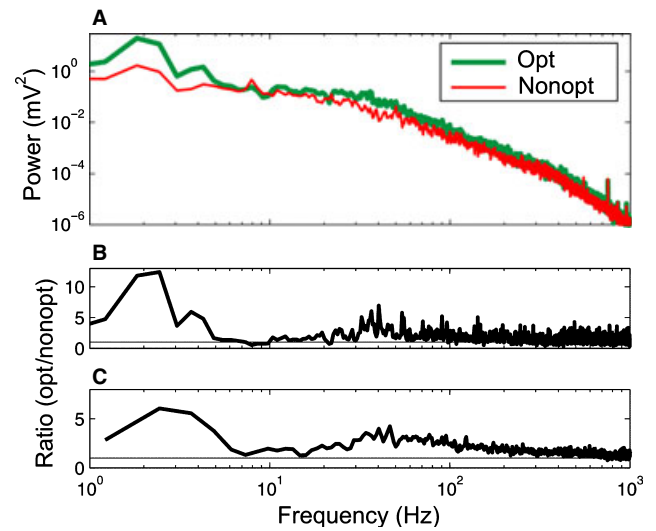


FIG. 2. Power spectra of the membrane potential responses to the optimal and non-optimal orientations of neurons, recorded in cat visual cortex. (A) Power spectra of the membrane potential responses of the cell from Fig. 1 to the optimal (green/gray thick line) and non-optimal (red/black thin line) orientations. (B) Ratio between the power spectra of responses to the optimal and non-optimal orientation; data from A. (C) Cumulative ratio of averaged power spectra of responses to the optimal and non-optimal orientation for nine neurons. To calculate the cumulative ratio, power spectra from nine cells for the optimal orientation were averaged, and divided by the averaged power spectrum for non-optimal responses. For interpretation of references to color in the figure legend, please refer to the Web version of this article.

around the temporal frequency of stimulation and up to approximately 5 Hz. The integral of the power spectrum in the range of stimulus frequency ± 0.5 Hz (1.5–2.5 Hz for this neuron) will be referred to as stimulus power. Second, the power of the high-frequency membrane potential fluctuations, especially in the γ -frequency range (25–70 Hz), was clearly stronger during the optimal stimulation. The difference in both the low-frequency and the high-frequency ranges stands out clearly in Fig. 2B, in which the ratio of the two power spectra is plotted. The difference between the optimal and non-optimal responses in the two frequency ranges was typical for our sample, as illustrated by two clear peaks around the stimulus power and the γ -power on the ratio of averaged power spectra for nine neurons (Fig. 2C).

Responses to the optimal and non-optimal orientations showed the most pronounced differences, as summarized in Table 1 for the cell from Figs 1 and 2. Stimuli of other orientations evoked responses with intermediate characteristics. As reported in previous studies (Carandini & Ferster, 2000; Volgushev *et al.*, 2000; Azouz & Gray, 2003, 2008), spike responses showed a sharper orientation tuning than slow modulation of the membrane potential at the temporal frequency of stimulation (Fig. 3A and D). Orientation tuning of the γ -power and its correlation with the amplitude of stimulus-induced slow membrane potential fluctuation had a similar shape to the tuning curves of the membrane potential and spike responses, although, unlike the firing rate and stimulus power, γ -power and its correlation did not fall to close to zero values even for a non-optimal range of orientations (Fig. 3B and C). The information rate was maximal in the firing evoked by optimal stimuli, and its orientation tuning essentially reproduced the tuning of spike responses (Fig. 3D and E).

Also in all other analyzed cells, stimuli of the optimal range, as defined by the maximal spike responses, evoked the strongest modulation of the membrane potential in the low-frequency and high-frequency ranges, and induced the strongest correlations

TABLE 1. Characteristics of membrane potential response, spike response and information rate assessed in cat visual cortex neuron *in vivo* and simulated with a model

	Optimal orientation		Non-optimal orientation		Null direction	
	Neuron	Model	Neuron	Model	Neuron	Model
Stimulus power (mV^2)	33.7	33.5	3.9	3.72	9.42	9.49
γ -Power (mV^2)	4.78	4.80	1.92	1.92	2.68	2.74
Correlation – γ /stimulus (r)	0.67	0.67	0.40	0.40	0.47	0.45
Firing rate (Imp/s)	16.9	17.2	0.29	0.95	6.2	3.10
Information rate (bits/s)	6.12	6.06	0.13	0.51	3.39	1.80

Responses of the neuron from Figs 1–3, 7, and 8. Responses simulated with this model are shown in Figs 4–6, and as red lines and diamond symbols in Figs 7 and 8. For both neuron and model, the stimulus was a moving sinusoidal grating at 2 Hz. Stimulus power was measured at the temporal frequency of stimulation, ± 0.5 Hz (1.5–2.5 Hz); γ -power, 25–70 Hz.

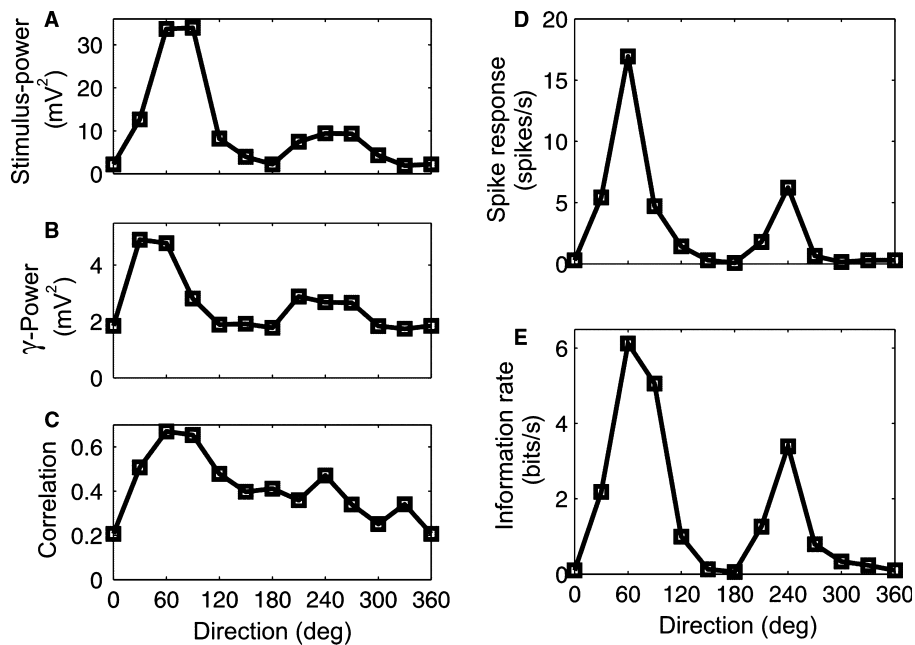


FIG. 3. Dependence of the response properties of the visual cortex neuron on the direction of movement of grating stimuli. Data are for the cell shown in Fig. 1. (A) Stimulus power (1.5–2.5 Hz) of the membrane potential. (B) γ -Power (25–70 Hz) of the membrane potential. (C) Linear correlation coefficient between the power of the γ -range fluctuations and the amplitude of the low-frequency fluctuations of the membrane potential. (D) Spike response. (E) Information rate.

between the γ -range power and the amplitude of the low-frequency membrane potential modulation. The information rates were also maximal during the responses to optimal stimuli. Table 2 summarizes the characteristics of responses to optimal, non-optimal (orthogonal orientation) and null (optimal orientation, but opposite direction of movement) stimuli for nine neurons. We observed a more than 10-fold difference in firing rates and information transfer rates between the responses to optimal and to non-optimal stimuli. A several-fold difference was observed between the optimal and non-optimal responses in the strength of the low-frequency (stimulus power) and the high-frequency (γ -power) membrane potential fluctuations. Furthermore, the γ -power and its correlation (r) with the amplitude of low-frequency membrane potential modulation was approximately two-fold stronger during the responses to optimal stimuli. In the following sections, we will use these values and their ranges as guidelines to construct a model neuron that reproduces experimentally observed values, and as benchmarks with which simulation results will be compared.

Construction and tuning of input conductances in the model neuron

Having quantified the properties of the membrane potential traces during responses to different orientations in the recorded neurons, we constructed input conductances that reproduced these features in a model neuron. The aim of tuning the input conductances was to create a model that reproduces the following characteristics of the measured neuronal responses: (i) spectral composition of the membrane potential fluctuations; (ii) averaged firing rate; (iii) dependence of the low-frequency modulation of the membrane potential on stimulus orientation/direction of movement; (iv) dependence of the high-frequency fluctuations on stimulus orientation; and (v) the relationship between low-frequency and high-frequency fluctuations of the membrane potential. This model will be used in the next part of this article to study how the low-frequency and high-frequency components of the input conductance contribute to the membrane potential responses, spike responses and information rate in neurons' firing.

TABLE 2. Average values and SDs of response characteristics for nine cat visual cortex neurons

	Optimal orientation		Non-optimal orientation	Null direction
	Neurons	Model	Neurons	Neurons
Stimulus power (mV ²)	18.4 ± 9.4	18.9	3.7 ± 3.5	8.9 ± 5.9
γ -Power (mV ²)	2.66 ± 1.91	2.71	0.95 ± 0.65	1.8 ± 1.54
Correlation – γ /stimulus (<i>r</i>)	0.61 ± 0.15	0.66	0.36 ± 0.12	0.48 ± 0.15
Firing rate (Imp/s)	14.1 ± 11.9	14.5	1.1 ± 1.6	4.8 ± 3.6
Information rate (bits/s)	5.7 ± 2.4	5.64	0.5 ± 0.8	2.7 ± 2.0

Characteristics of optimal responses and their variation were used as benchmarks for simulations for Figs 9 and 10. Column ‘Model’ gives values for simulated optimal responses.

Fluctuating conductance input, which reproduces in the model the above properties of membrane potential traces recorded in visual cortex neurons *in vivo*, was constructed in several steps. We first generated excitatory and inhibitory input conductances that induced membrane potential fluctuations with a spectral composition similar to the spectrum of the membrane potential recorded in a neuron during presentation of a moving grating with optimal orientation. To the fluctuating input conductances, we added sinusoidal modulation representing the stimulus, additional fluctuations in the γ -band, modulation of their power by the stimulus, and a constant current component that was used to control the mean depolarization level of the membrane potential. As these added conductances changed the spectral composition of the membrane potential fluctuations, the initial spectral composition and all other parameters were then fine-tuned to fit experimental data. Below, we describe these steps in detail.

The excitatory $g_e(t)$ and inhibitory $g_i(t)$ fluctuating input conductances with which the spectral composition of membrane potential traces recorded in neurons was reproduced were generated as follows. First, we generated a Gaussian white noise, transferred it to Fourier space, and multiplied it component-wise with a function $f(\omega)$:

$$f(\omega) = a_1 \exp(-\tau_1 \omega) + a_2 \exp(-\tau_2 \omega) + a_3 \exp(-\tau_3 \omega), \quad (6)$$

The result was then transferred back to the time domain with an inverse Fourier transformation. In the function $f(\omega)$, the parameters a_1 – a_3 and τ_1 – τ_3 represent three frequency ranges: low (0–25 Hz), gamma (25–70 Hz), and high (70–1000 Hz). One of the effects of changing orientation of the moving grating on neuronal response is alteration of the relative contributions of low-frequency and γ -band frequency fluctuations of the membrane potential. The function $f(\omega)$ allowed us to account for the differential contribution of these frequency bands to neuronal responses with different orientations by adjusting the respective coefficients.

Visual stimulation was simulated by adding sinusoidal components to the excitatory and inhibitory conductances. The total synaptic conductances $g_e(t)$ and $g_i(t)$ of Eqn (3) are then given by:

$$\begin{aligned} g_e(t) &= \bar{G}_e + g_{es} \sin(2\pi ft) + g_{e0}(t) \\ g_i(t) &= \bar{G}_i + g_{is} \sin(2\pi ft) + g_{i0}(t) \end{aligned} \quad (7)$$

where G_e and G_i are the mean excitatory and inhibitory conductances, g_{es} and g_{is} determine the strength of modulation of excitatory and inhibitory conductance by the stimulus, which was a moving grating with a temporal frequency f (e.g. $f = 2$ Hz), and $g_{e0}(t)$ and $g_{i0}(t)$ represent the fluctuating excitatory and inhibitory background conductances.

Next, we implemented specific details of the γ -band fluctuations of the membrane potential – their generation by the interaction of excitatory and inhibitory conductances (Bringuier *et al.*, 1997; Lampl *et al.*, 1999; Cunningham *et al.*, 2004; Hasenstaub *et al.*, 2005; Bartos *et al.* 2007; Sohal *et al.*, 2009), and co-variation of the power of the γ -range fluctuations with the amplitude of the slow modulation of the membrane potential by the stimulus (see above). We used the following procedure. First, the excitatory conductance trace $g_e(t)$ (see Eqn 7) was segregated in Fourier space into two frequency components. The first component, $g_{e\gamma}(\omega)$, contained the frequencies in the γ -range (25–70 Hz), and the second component, $g_{e,rest}(\omega)$, contained all remaining frequencies (< 25 and > 70 Hz). To account for the increased power of the γ -range fluctuations during visual stimulation,

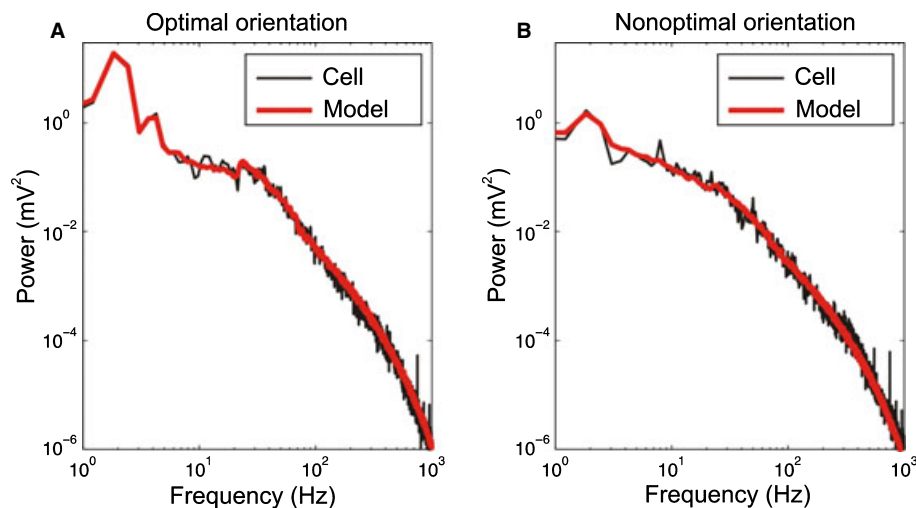


FIG. 4. Power spectra of the membrane potential responses to optimal (A) and non-optimal (B) orientation in the recorded cell (thin black lines, the neuron from Fig. 1) and in the model neuron (thick red/gray lines). For interpretation of references to color in the figure legend, please refer to the Web version of this article.

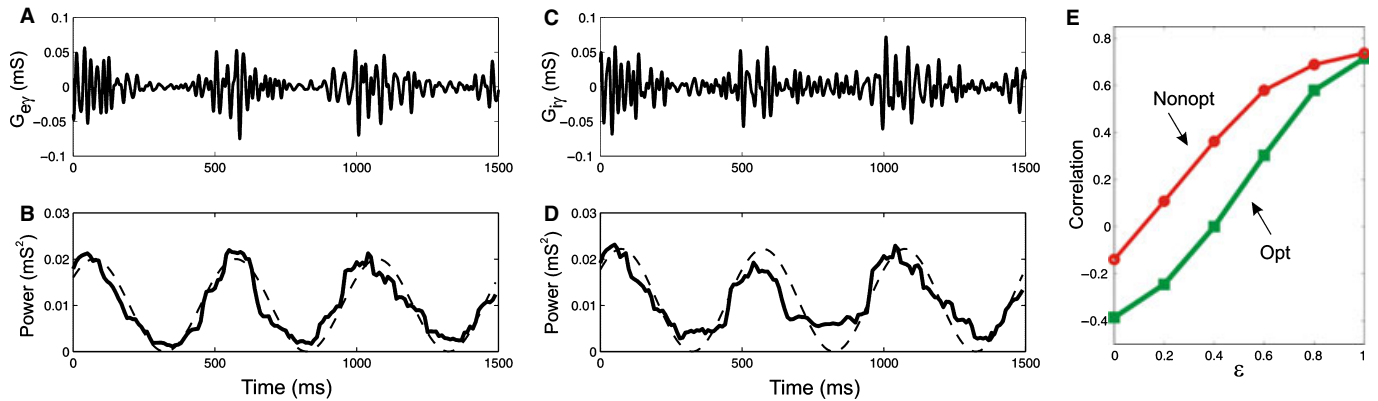


Fig. 5. Modulation of the γ -range conductance in the model neuron. (A and C) γ -Range component (25–70 Hz) of the excitatory (A) and inhibitory (C) conductance traces with strong ($\varepsilon = 1$) modulation. (B and D) Relationship between the expected modulations of the γ -power of the excitatory and inhibitory conductances (dashed lines) and the γ -power calculated from the trace in A and C (thick lines), using a running window of 102.4-ms duration. (E) Linear coefficient of correlation (r) between the amplitude of the γ -range fluctuations and the slow changes in the membrane potential in the model neuron plotted against the strength of modulation of γ -range conductances (ε) for responses to a strong (optimal, green/gray line, squares) and a weak (non-optimal, red/black line, circles) stimulus. For interpretation of references to color in the figure legend, please refer to the Web version of this article.

Fourier coefficients in the γ -range were multiplied by $1 + \gamma_c * F(\omega)$, where γ_c was an adjustable coefficient, and $F(\omega)$ was a fixed, exponentially decaying function. The amplitude of the γ -range component of the excitatory conductance was modulated with a sinusoidal signal at the temporal frequency of the stimulus f (Eqn 8). Then, the γ -range component of the excitatory conductance, but taken with an opposite sign and multiplied by c_γ ($c_\gamma = 1$ for the optimal orientation; $c_\gamma = 0.3$ for the non-optimal orientation), was added to the inhibitory conductance (Eqn 8). For a single-frequency oscillation (e.g. a sine-wave), this would be equivalent to an anti-phase relationship between the excitatory and inhibitory processes. The respective modulated γ -band signals were then added to excitatory and inhibitory conductances $g_{e,rest}(t)$ and $g_i(t)$ to yield the total conductances $g_{e0}(t)$ and $g_{i0}(t)$:

$$\begin{aligned} g_{e0}(t) &= g_{e,rest}(t) + \beta \left(1 + \frac{\varepsilon}{2} \sin(2\pi ft) - \frac{\varepsilon}{2} \right) g_{e\gamma}(t) \\ g_{i0}(t) &= g_i(t) - c_\gamma \beta \left(1 + \frac{\varepsilon}{2} \sin(2\pi ft) - \frac{\varepsilon}{2} \right) g_{e\gamma}(t) \end{aligned} \quad (8)$$

in Eqn (8), ε determines the degree of modulation ($0 < \varepsilon < 1$, so that with $\varepsilon = 0$, the γ -range component is unmodulated, and $\varepsilon = 1$ corresponds to the maximal modulation). As the modulation affects the standard deviation (SD) of $g_{e0}(t)$ and $g_{i0}(t)$, we included an additional parameter, β , that allowed to compensate for the change of the SD of $g_{e0}(t)$ and $g_{i0}(t)$, and a coefficient, c_γ , that allowed a scaling between the excitatory and inhibitory γ -range conductances. These coefficients allowed us to bring the SD back to the same value as in the original trace without modulation.

The influences of the above components of input conductances on the membrane potential fluctuations are not independent of each other. For example, low-frequency stimulus modulation of the input and modulation of the γ -band fluctuations changed the overall frequency composition of the membrane potential fluctuation, and thus their power spectrum. Therefore, additional adjustment of input parameters was necessary to reproduce multiple characteristics of measured neuronal responses in the model. This fine-tuning was achieved by repeating the above steps while adjusting the input conductances until the parameters of simulated responses matched the parameters of responses measured in cat neurons *in vivo* with a deviation of $< 3\%$.

Figure 4 shows power spectra of the simulated voltage traces (solid red/gray lines), superimposed on the power spectra of recorded membrane potential traces (thin black lines), for the optimal and non-optimal responses. A close correspondence between the simulated and the recorded spectra illustrates that the spectral composition, as well as the difference between the optimal and non-optimal responses, was reproduced well in the simulations. Adjustment of the coefficients a_1 – a_3 and τ_1 – τ_3 of the function $f(\omega)$ in Eqn (6) to reproduce the frequency spectra of recorded data was performed only for optimal and non-optimal orientations. These coefficients are listed in Table 3. For all other orientations, the coefficients were linearly interpolated according to the measured orientation/direction tuning of neuronal responses.

Figure 5A–D shows a sample trace of the γ -frequency component of the excitatory and inhibitory conductances $G_{e\gamma}(t)$ and $G_{i\gamma}(t)$, with strong modulation ($\varepsilon = 1$) of the amplitude of the γ -range fluctuations. In Fig. 5B and D, the running average of the γ -power in the excitatory (Fig. 5B) and inhibitory (Fig. 5D) conductances (thick solid line), calculated in a sliding window of 102.4 ms, is compared with the expected modulation of the γ -power (thin dashed line). The measured modulation of the γ -power is in good agreement with expectations. However, even the strongest ($\varepsilon = 1$) modulation of the γ -power of the input conductance led to a correlation of < 1 between the amplitude of the γ -range fluctuations and the slow depolarizations of the membrane potential ($r = 0.72$ for the example in Fig. 5). Apart from the noisy nature of the simulated input and low-pass filter property of the neuron, two more factors contributed to the reduction of the correlation in the membrane potential trace as compared with the actual modulation of the input conductance – the calculation procedure and mutual shunting of different conductances. The estimate of the correlation coefficient depends on the duration of the sliding window used for the calculation of the running average of the γ -power. Too short a window gives unreliable estimates of the γ -power, and for too long windows the assumption of constant stimulus does not hold. With the stimulation frequencies used in our study (0.5–2.5 Hz in different neurons, optimized for each cell), maximal values were obtained with a running window of about 100-ms duration. However, even with this optimal window length, the correlation coefficient was 0.72 for a perfectly correlated signal.

One further factor contributing to the reduction of the correlation in the membrane potential traces is a shunting effect of the slow

TABLE 3. Parameters used to simulate synaptic conductance $I_{\text{syn}}(t)$ – stimulus conductance g_s , mean background conductance G and parameters of the filter $f(\omega)$ for generation of the excitatory and inhibitory fluctuating conductances $g_{e0}(t)$ and $g_{i0}(t)$ (see Eqns 3, 6 and 7)

	Model parameters used in simulations for Figs 4–8				Model parameters for Figs 9 and 10	
	Optimal orientation		Non-optimal orientation		Optimal orientation	
	Excitatory	Inhibitory	Excitatory	Inhibitory	Excitatory	Inhibitory
g_s (mS/cm ²)	0.1	0.015	0.023	0.0035	0.08	0.012
G (mS/cm ²)	0.119	0.135	0.125	0.12	0.142	0.115
a_1	1.3	0	0.95	0	1.45	1
a_2	0.45	0.15	0.35	0.15	0.24	0.15
a_3	0.133	0.1	0.095	0.1	0.091	0.1
τ_1 (ms)	400	0	200	0	220	220
τ_2 (ms)	50	50	50	50	50	50
τ_3 (ms)	2.2	2	2.2	2	2	1.5

changes of the input conductance and thus of the input resistance of the neuron at the temporal frequency of stimulation. During the positive, depolarizing phase of the response to stimulation, when the γ -range conductances have higher amplitudes, the total input conductance is also larger, leading to stronger shunting. As a result, high-amplitude γ -range conductances will be subject to stronger reduction by shunting during the translation into membrane potential fluctuations than low-amplitude γ -range conductances. Thus, low-frequency, stimulus-induced modulation of the input conductance counteracts the modulation of the amplitude of the γ -range fluctuations. Figure 5E illustrates the relationship between the conductance modulation (ε) and measured correlation (r) between the γ -power and slow depolarizations in the membrane potential for the strong (e.g. optimal; green/gray line, square symbols) and weak (e.g. non-optimal; red/black line, circles) responses. Figure 5E shows that strong stimulation has a stronger reducing effect on the measured correlation, and at low ε can lead even to negative values of the correlation coefficient.

Figure 6 illustrates membrane potential traces simulated with the model neuron for optimal (Fig. 6A–C) and non-optimal (Fig. 6D–F) orientation and their analysis, which was performed in exactly the same way as the analysis of intracellular recordings in visual cortex neurons (see Fig. 1). The simulated traces reproduce well the properties of those recorded. The simulated and the recorded responses have similar amplitudes of the slow modulation and the γ -range fluctuations of the membrane potential, as well as the correlation between the γ -power and the amplitude of the slow modulation (Table 1). To obtain in the membrane potential traces the values for correlation coefficient similar to those observed in the experiment, we had to introduce strong conductance modulation ($\varepsilon = 0.9$) for the optimal response. At non-optimal orientation, a lower value ($\varepsilon = 0.4$) was sufficient to reproduce the correlation seen in the experimental data.

Despite a clear overall similarity with the recorded membrane potential responses, the simulated traces have slightly different shapes of the slow depolarizations. In the simulations, the depolarization peaks are somewhat broader, owing to a cut-off, which occurred because a substantial part of the stimulus was suprathreshold. The correspondence of the shape of depolarization peaks with the recordings could have been recovered by decreasing the average membrane potential. However, this would also lead to a substantial

reduction of the average firing rate of the model neuron. As stimulus encoding depends strongly on firing rate, we opted for obtaining in the simulations similar firing rates, but slightly deviating from the recorded shapes of the slow depolarizations.

γ -Range membrane potential fluctuations and stimulus encoding in the model neuron

Using the neuron model described above, we studied how orientation tuning of spike responses and neuronal coding is influenced by: (i) the high-frequency membrane potential fluctuations; (ii) dependence of their strength on stimulus optimality; and (iii) modulation of their amplitude by slow membrane depolarizations. To this end, we simulated and analyzed responses to stimuli with different orientations/directions of movement for three classes of input. In the first class, only the low-frequency stimulus power was adjusted to fit the experimentally observed values. This class will be referred to as ‘stimulus alone’. In the second class, in addition to the stimulus power, the γ -power increase with stimulus optimality was also implemented. In this class, ‘unmodulated gamma’, the γ -power was adjusted to the experimentally observed values, but was not modulated with the slow membrane depolarizations ($\varepsilon = 0$). In the third class, ‘modulated gamma’, in addition to the stimulus and γ -power, the modulation of the amplitude of the γ -range fluctuations by slow membrane depolarizations was also adjusted to the experimental values. For this latter adjustment, we used ε -values between 0.2 and 0.9 ($0.2 < \varepsilon < 0.9$), so that the correlation coefficients calculated for the simulated responses were similar to the experimentally observed values (0.67 vs. 0.66 for the optimal orientation, and 0.40 vs. 0.39 for the non-optimal orientation; see also Fig. 7C).

Orientation tuning of the model neuron

Figure 7 shows orientation tuning of different parameters in the model neuron for the three classes of input (three solid lines, color coded), and compares the simulations with the data from the recorded visual cortex neuron (black dashed line). The results presented in Fig. 7 demonstrate that the three classes of model input reproduced well the implemented properties of membrane potential fluctuations and their orientation tuning. All three model inputs precisely reproduced the low-frequency modulation of the membrane potential at the temporal frequency of stimulation, as indicated by an almost complete overlap of the simulation results and experimental data in Fig. 7A. Orientation tuning of the γ -power (Fig. 7B) was faithfully reproduced by the complete input model (red line in Fig. 7B) and by the unmodulated gamma input model (green line in Fig. 7B), but not by the stimulus alone input (blue line in Fig. 7B). Finally, only the complete input model reproduced orientation tuning of the correlation between the γ -power and the amplitude of low-frequency membrane potential modulation (Fig. 7C, red line). With the two other model inputs, correlation coefficients were well off the measured values (Fig. 7C, green and blue lines).

Figure 7D shows the spike tuning of the recorded cell and the three models. Orientation tuning of spike responses in the model neuron with the modulated gamma input reproduced the tuning of the recorded cell most closely (Fig. 7D, red line for the model, and black dashed line for the visual cortex neuron). Some minor deviations of the simulated spike response from the experimental data were attributable to the fact that, in the recorded cell, the mean membrane potential was also changing as a function of stimulus orientation. This dependence was not implemented in the model. Furthermore, direction

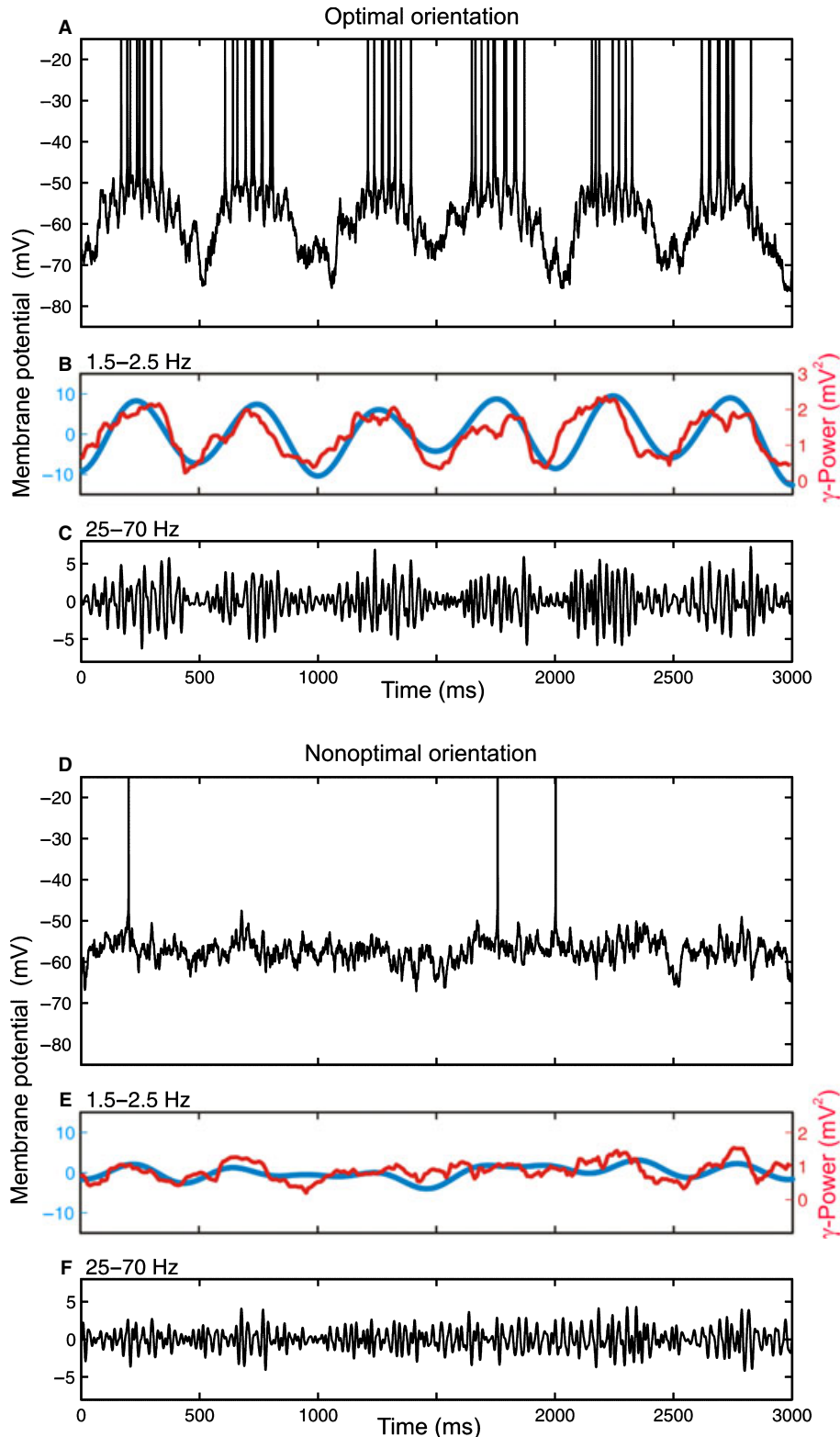


FIG. 6. Simulated responses of the model neuron to optimal (A) and non-optimal (D) orientation and their analysis. The spectral composition of the simulated traces was adjusted to match the spectral composition of the responses recorded in the cell in Fig. 1. (A and D) Simulated membrane potential traces. The temporal frequency of the moving grating was 2 Hz. Action potentials are truncated. (B, C, E and F) Analysis of the relationship between the low-frequency component (1.5–2.5 Hz, blue/gray lines in B and E, scale on the left) and the high-frequency, γ -range component (25–70 Hz, C and F) from the traces in A and D. In B and E, red/black lines (scale on the right) show the power of the γ -range fluctuations estimated in a running window of 102.4 ms. Note that the γ -power curves are scaled to match the amplitude of the respective low-frequency components. For interpretation of references to color in the figure legend, please refer to the Web version of this article.

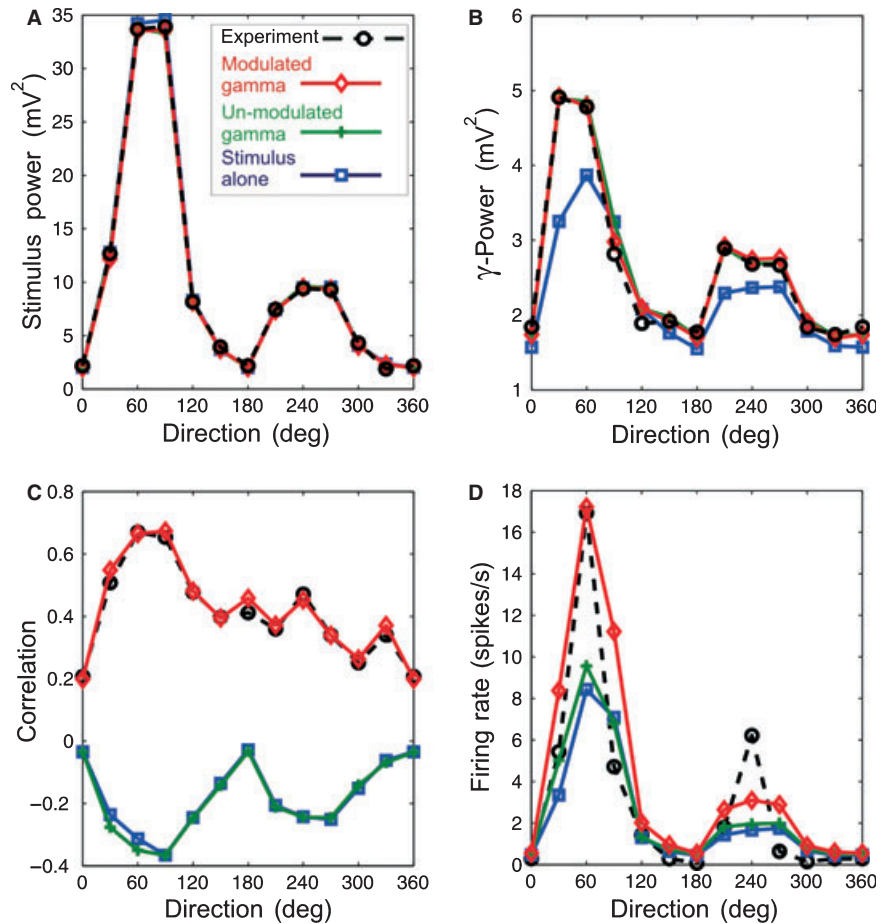


FIG. 7. Comparison of the features of the neuronal responses in cat visual cortex *in vivo*, and of the simulated responses in the model neuron, which received inputs of three different classes. In A–D, circles and black dashed lines show recorded data (neuron from Fig. 1). Simulated data are shown in different colors for the three types of input. Blue lines, squares – stimulus alone input, with only stimulus power adjusted to fit the experimental data. Green lines, crosses – unmodulated gamma input, in which, in addition to the stimulus power, the γ -power depended on stimulus optimality. Red lines, diamonds – modulated gamma input, in which, in addition to the stimulus and γ -power, the modulation of the amplitude of the γ -range fluctuations by slow membrane depolarizations was adjusted to the experimental values. All response features are plotted against the direction of grating movement. (A) Strength of the low-frequency fluctuations of the membrane potential (stimulus power). (B) γ -Power of the membrane potential responses. (C) Correlation between the stimulus power and the γ -power. (D) Spike count.

selectivity may involve enhancement of responses to stimuli of optimal orientation by mechanisms of facilitation or disinhibition, which were also not implemented here. These factors or their combination might be responsible for the small difference between the real neuron and the model in firing rates at null orientation. In the simulations without modulation of the γ -power (unmodulated gamma, green cross line), the model neuron generated considerably fewer spikes, although all other parameters of simulation remained unchanged (Fig. 7A–C). With the unmodulated gamma input model, the firing rate in response to optimal orientation was only about 60% of that in the recorded neuron or in the model with γ -power modulation. Note that this model did not reproduce the experimentally observed correlation between the membrane depolarization and the amplitude of γ -fluctuations (Fig. 7C). For most orientations, this correlation was even negative, because of the shunting effect of the stimulus conductance. Because of the shunting, the amplitudes of unmodulated γ -range fluctuations were most strongly reduced during strong depolarizations, leading to the negative correlation (see Fig. 5 and related text above).

Analysis of spike responses obtained with the third class of model inputs (stimulus alone, blue square line in Fig. 7) revealed their similarity to the unmodulated gamma model, indicating that the adjustment of unmodulated γ -power to the experimentally observed value had only a small effect on the firing rate. Orientation tuning curves of the model neurons' firing generated in response to unmodulated gamma input or the stimulus alone input were very similar (Fig. 7D, blue and green lines). Interestingly, even in the stimulus alone model, the γ -power increased with stimulus optimality. This increase was clearly

smaller than with other input models (Fig. 7B, blue line), and was attributable to the fact that, in the model, the power spectra of the membrane potential traces for different orientations were generated from the optimal and non-optimal spectra by linear interpolation (see above,

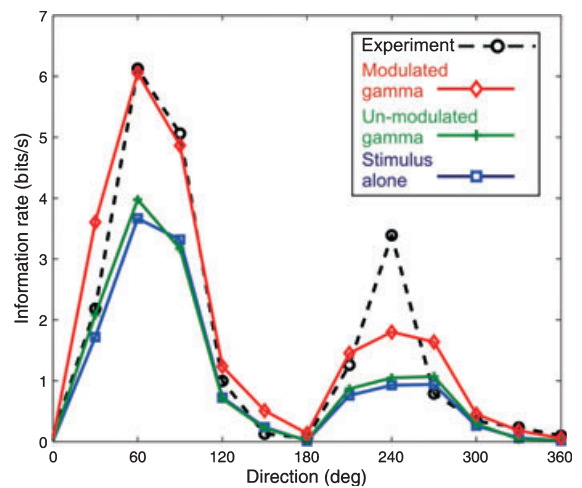


FIG. 8. Comparison of the information rates in the recorded and simulated responses. Circles and black dashed lines – recorded data, neuron from Fig. 1. Simulated data are shown in different colors for the three types of input, as in Fig. 7. Blue lines, squares – stimulus alone input. Green lines, crosses – unmodulated gamma' input. Red lines, diamonds – 'modulated gamma' input. Information rate is plotted against the direction of grating movement.

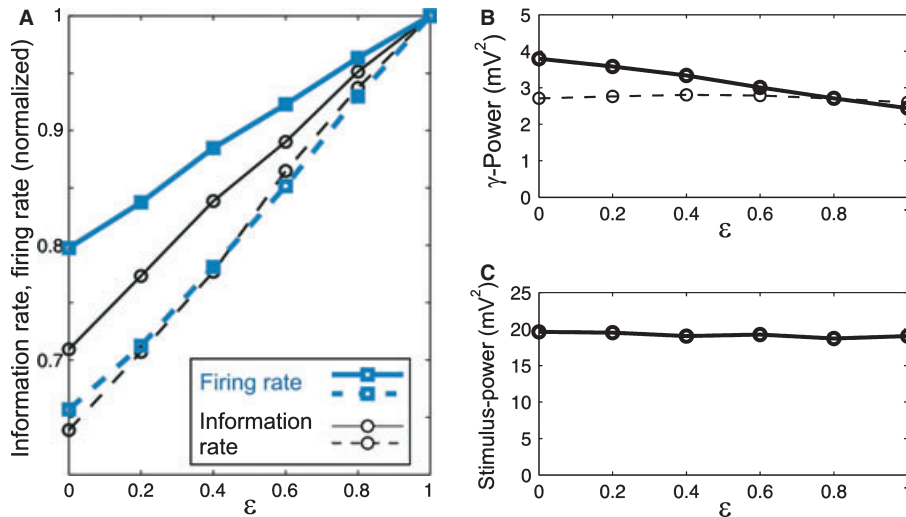


FIG. 9. Dependence of the information rate, the firing rate, the high-frequency (γ -range) power and the low-frequency (stimulus) power in the model neuron on the degree of modulation of the γ -band activity by the low-frequency changes in the membrane potential (ϵ). (A) Information rate (black lines) and firing rate (blue lines) plotted against the degree of γ -band activity modulation in the model neuron with (dashed lines) and without (continuous lines) keeping the total γ -power constant. Decrease of ϵ reduces both information rate (thin, black solid curve, circles) and firing rate (thick, blue solid curve, squares). The dashed lines show the corresponding values for the information rate and firing rate in a model in which the γ -band activity was kept constant at different values of ϵ . Information rate and firing rate are normalized to one at $\epsilon = 1$. (B) γ -Power of the membrane potential plotted against the degree of γ -band activity modulation ϵ (thick solid curve). The thin (dashed) curve represents the γ -power of V_m for simulations, where the γ -power was adjusted to match the experimentally observed mean value (see Table 2). (C) Stimulus power plotted against the degree of γ -band activity modulation.

Fig. 4 and related text). However, in both the unmodulated gamma and the stimulus alone model inputs, γ -range fluctuations were most strongly reduced by shunting during strong depolarizations, as indicated by the negative correlation between γ -power and slow depolarization amplitude (Fig. 7C, blue and green lines). The shunting by strong depolarizations, that is, at those moments when the membrane potential was closest to the firing threshold, made γ -range fluctuations in these two models less effective in driving spikes.

Differences between responses of the model subjected to three kinds of input allow us to make inferences regarding the contribution of the γ -range fluctuations to stimulus encoding (Fig. 8). The information

rate was highest in those simulations that included the modulation of the amplitude of the γ -range fluctuations (red curve). At optimal orientation, the estimated information rate for the model neuron was same as for the cell (6.06 vs. 6.12 bits/s). For the null direction of movement, the information rate in the model was slightly lower than in the recorded cell (1.8 vs. 3.39 bits/s), because of the lower firing rate (3.1 vs. 6.21 spikes/s). In the models without modulation (blue square and green cross curves), the information rate was clearly lower than with modulation, which was an expected consequence of the lower firing rates. Moreover, both models without γ -power modulation had essentially the same information rates, showing that addition of

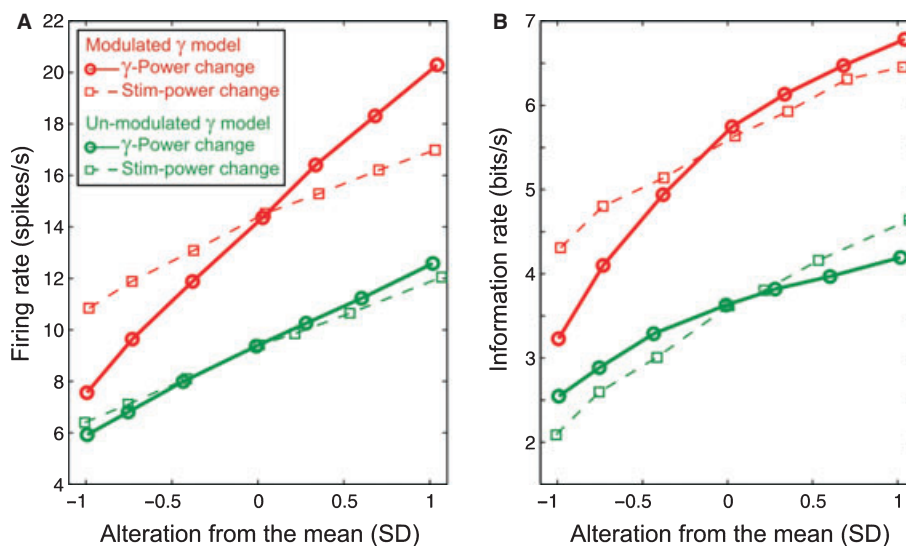


FIG. 10. Dependence of the firing rate (A) and the information rate (B) on alteration of the stimulus power (dashed lines, squares) or the γ -power (solid lines, circles). Both the stimulus and the γ -power were altered by ± 1 SD from the mean values measured in visual cortex neurons *in vivo* (see Table 2). Red lines – model with complete modulation of the γ -power by slow membrane depolarizations ($\epsilon = 1$). Green lines – model with unmodulated γ -power.

unmodulated γ -range fluctuations of the membrane potential has little effect on encoding. Thus, information encoding is improved only by modulated γ -range fluctuations, whereby higher information rates result from the ability of the modulated γ -range fluctuations to facilitate stimulus-locked firing of neurons.

Note that for the two models without γ -power modulation, similar firing rates (and information rates) could have been achieved by some other mechanism, for example by raising the average membrane potential of the model neuron. However, we will show in the following that modulation of the γ -power is a most efficient mechanism for regulation of stimulus encoding.

γ -Activity modulation and stimulus encoding

To investigate further the effect of the γ -activity modulation on stimulus encoding, we used the most complete model, with stimulus-dependent low-frequency modulation, stimulus-dependent γ -power modulation and depolarization-dependent modulation of the γ -activity. In this model, we systematically changed the strength of the depolarization-dependent modulation of the γ -activity, while adjusting all other parameters to match the averaged values of optimal responses in our experimental data sample (Table 2). Stimulus conductance g_s , the mean background conductance G and the parameters of the filter function $f(\omega)$ (see Eqns 6 and 7) used to reproduce these responses are listed in Table 3.

Dependency of the information rate and the firing rate on the strength of the γ -power modulation by the amplitude of slow membrane depolarizations (ε) is shown in Fig. 9. A decrease of the modulation of γ -range conductance (ε) leads to decreases in both the information rate and firing rate (Fig. 9A, solid lines). Interestingly, with decreasing ε , the firing rate decreases more slowly, reaching 80% at $\varepsilon = 0$ (thick line, square symbols) than the information rate, which falls to 71% at $\varepsilon = 0$ (thin line, circles). The slower decrease in the firing rate may result from the fact that decrease in ε actually leads to an increase in the total power of the γ -range fluctuations of the membrane potential, as illustrated in Fig. 9B (thick solid line). When the amplitude of the γ -range fluctuations is strongly correlated with depolarization peaks ($\varepsilon = 1$), the γ -range fluctuations are subjected to strong shunting by the stimulus-induced high conductance. With decreasing correlation ($\varepsilon < 1$), the power of the γ -range fluctuations of the excitatory conductance becomes distributed more evenly between the phases of stronger and weaker stimulus-induced depolarizations, and the γ -range fluctuations are therefore less shunted by the stimulus conductance. As a result, the total power of the membrane potential fluctuations in the γ -band increases with decreasing ε . This increase in the total γ -band power of the membrane potential fluctuations explains the slower decrease in the firing rate in Fig. 9A. Adjusting the amplitude of the γ -range fluctuations in the model, such that the total γ -power of the membrane potential fluctuations remained the same at all values of ε (Fig. 9B, dashed line), resulted in both the firing rate and the information rate decreasing more substantially, but also more uniformly, with decreasing ε (Fig. 9A, dashed lines, squares for information rate, circles for firing rate).

Changing the degree of modulation of the γ -power by the slow membrane depolarizations had only a small influence on stimulus power (Fig. 9C). A minor increase in stimulus power with decreasing ε can be attributed to redistribution of the γ -activity. With decreasing ε , some of the γ -range conductance is shifted away from the depolarization peaks, leading to weaker shunting of the depolarization peaks, first by the γ -range conductance itself, and second by action potential-related conductances, as fewer spikes are generated at depolarization peaks.

Factors influencing firing rate and stimulus encoding

The information rate depends (i) on firing rate, because each additional spike contains some information about the stimulus, and (ii) on the information content of each action potential, that is, the precision of its relationship with the stimulus. Thus, stimulus encoding may be changed by varying either the firing rate or the precision of the spiking. In the next series of simulations, we investigated how the firing rates and stimulus encoding are affected by variation of the amplitude of the slow modulation of the membrane potential at the temporal frequency of the stimulus, and by variation of the power of the membrane potential fluctuations in the γ -range. For both of these parameters, we used the ranges of variability seen in the experimental data, and modified them by ± 1 SD from the mean (see Table 2). The alteration in stimulus or γ -power in the range of ± 1 SD of the experimentally observed values was achieved by varying either the stimulus conductance g_s (stimulus power) or the parameter γ_c (γ -power); see Eqns 7 and 8 and related descriptions.

We compared the behavior of two models, the first one with complete modulation of the γ -range power by slow membrane depolarizations ($\varepsilon = 0.85$, which yields the correlation $r = 0.61$, observed in experimental data for optimal orientation), and the second one with unmodulated γ -range activity ($\varepsilon = 0$).

In Fig. 10A, the firing rate is plotted against the changes in the stimulus power or the γ -power. In both models, alteration of either the stimulus or the γ -range power led to changes in the firing rate. However, the firing rate was affected most strongly by changing the γ -power in the complete model with the slow depolarization-modulated γ -range activity. In the complete model (Fig. 10A, red solid line, circles), changing the γ -power by ± 1 SD from the mean changed the firing rate over the range from 7.6 to 20.3 spikes/s, or approximately 6.4 spikes/s per SD. Changing the stimulus power in the same model led to a firing rate change over a smaller range, from 10.8 to 17 spikes/s or approximately 3.1 spikes/s per SD (Fig. 10A, red dashed line, squares). In the model with unmodulated gamma, both the overall firing rates and the range of their changes were lower (Fig. 10A, green lines). In this model, changes in the γ -power or the stimulus power modified firing rates over comparable ranges (from 5.9 to 12.6, or approximately 3.3 spikes/s per SD; and from 6.4 to 12, or approximately 2.8 spikes/s per SD).

Changes in the firing rate were associated with changes in the information rate in neuronal spiking. Dependences of changes in the information rate on the alteration of the stimulus power or the γ -power for the two models (Fig. 10B, same simulations as in Fig. 10A) demonstrate two important points. First, information rates were systematically higher in the model with the γ -range activity, modulated by the slow membrane depolarizations. This is illustrated by the fact that the red lines, which represent the data obtained with the modulated-gamma model, are located higher than the green lines, which represent data from the model with unmodulated gamma (Fig. 10B). Second, alteration of the γ -power in the model with modulated gamma had the strongest effect on stimulus encoding (Fig. 10B, thick red line, circles). The range of the information rate changes was from 3.2 to 6.7 bits/s, or approximately 1.78 bits/s per SD. This range was broader than those produced by altering the γ -power in the unmodulated gamma model (from 2.5 to 4.2 bits/s, or approximately 0.82 bits/s per SD; green solid line) or by altering the stimulus power [from 4.3 to 6.5 bits/s, or approximately 1.1 bits/s per SD for the modulated gamma model (red dashed line), and from 2.1 to 4.6 bits/s, or approximately 1.3 bits/s per SD for the unmodulated gamma model (green dashed line)].

The results shown in Fig. 10 demonstrate that alteration of the γ -band activity at the input to the neuron represents the most effective way of changing the firing rate and the stimulus encoding. To evaluate the statistical significance of this effect, we repeated simulations with a complete model (with γ -power modulation) 100 times, while varying either the γ -power or the stimulus power (both \pm SD). Varying the γ -power changed the firing rate by 12.7 ± 0.3 spikes/s ($n = 100$), whereas varying the stimulus power led to significantly smaller changes (6.3 ± 0.3 spikes/s, $P < 0.001$, one-sided t -test). Similarly, the information rate was influenced significantly stronger by varying the γ -power than by varying the stimulus power (3.5 ± 0.2 vs. 2.1 ± 0.22 bits/s, $P < 0.001$, $n = 100$).

Taken together, these results show that alteration of the γ -band activity at the input to the neuron represents the most effective way of changing the firing rate and the stimulus encoding, and that the model with modulated gamma provides the most efficient encoding of the stimulus.

Discussion

The main results of the present study are as follows. Analysis of intracellular recordings from visual cortex neurons showed that the difference between membrane potential responses to the optimal and non-optimal stimuli is most pronounced in two frequency ranges: at low frequencies around the temporal frequency of the stimulation, and at high frequencies, in the γ -range and above (25–200 Hz). Furthermore, the power of the γ -range fluctuations (25–70 Hz) correlated with the amplitude of the slow membrane potential modulation at the temporal frequency of the stimulus. Our simulations showed, that: (i) stimulus encoding was substantially improved by modulation of the γ -power by the amplitude of low-frequency changes in the membrane potential; (ii) changing the degree of modulation of the γ -activity by the low-frequency signal had clearly stronger effects on both the firing rates and information rates than changing the amplitude of the low-frequency stimulus itself; and (iii) unmodulated, uniform γ -activity led to only a moderate enhancement of the firing rates, information rates and improvement of encoding as compared with the stimulus-alone condition, in which only the amplitude of the low-frequency stimulus itself was varied.

Electrophysiological results

We selected for the analysis only visual cortex neurons with simple-type receptive fields, with clear modulation of the membrane potential and firing at the temporal frequency of the stimulation (Dean & Tollhurst, 1983; Skottun *et al.*, 1991; Carandini & Ferster, 2000; Volgushev *et al.*, 2003). Previous studies showed that γ -band fluctuations in the membrane potential constitute a common property of visual cortex neurons, being expressed in both simple and complex cells (Jagadeesh *et al.*, 1992; Gray & McCormick, 1996; Anderson *et al.*, 2000b; Volgushev *et al.*, 2002, 2003; Azouz & Gray, 2003, 2008). However, neurons with complex receptive fields do not encode in their firing the temporal frequency of the stimulus, and thus are not suited to the purposes of this study. In the simple cells, the amplitude of the γ -band fluctuations correlated with the amplitude of the slow, stimulus frequency modulation of the membrane potential, being maximal at depolarization peaks and minimal at hyperpolarization troughs of the membrane potential responses (Volgushev *et al.*, 2003). The results of the present study confirm and extend these findings. We have now used an improved measure of the relationship between the high-frequency fluctuations and the slow changes of the membrane potential – correlation between the low-frequency component and the running average of the power of the high-frequency fluctuations. This

measure has two advantages over the previously used envelope-based method: (i) it gives a better estimation of their relationship and higher correlation values; and (ii) it can be better formalized and thus used as a variable (and also as a constraint) in the simulations.

The results of this study confirm previous reports (Volgushev *et al.*, 2002, 2003; Azouz & Gray, 2003, 2008) that the difference in the spectral compositions of membrane potential responses to presentation of the optimal and non-optimal stimuli is most pronounced in two ranges of frequencies: the low (below 4 Hz) and the high (25–200 Hz). The difference between the optimal and non-optimal responses in the low-frequency range, around the temporal frequency of stimulation, is present in simple cells by definition. More interesting is that the difference becomes less pronounced at intermediate frequencies (5–20 Hz), but increases again by several-fold in the γ -band and higher-frequency range (25–200 Hz). The decreased difference in the middle range indicates that the stronger high-frequency fluctuations of the membrane potential during the optimal stimulation were not caused by high-order harmonics of the stimulation frequency. Rather, high-frequency fluctuations might reflect a genuine temporal structure of the input activity.

Previous research has demonstrated that the γ -band fluctuations can impose precise temporal windows for synaptic integration (Lampf & Yarom, 1993; Volgushev *et al.*, 1998; Azouz & Gray, 2003, 2008), make the generation of action potentials more reliable (Mainen & Sejnowski, 1995; Nowak *et al.*, 1997; Volgushev *et al.*, 1998, 2003; Salinas & Sejnowski, 2000; Azouz & Gray, 2003, 2008), and thus facilitate the generation of precise temporal patterns of activity (Mainen & Sejnowski, 1995; Nowak *et al.*, 1997). The stronger contribution of the γ -band fluctuations to the optimal response may indicate an interesting possibility that the high-frequency band is used to transmit the most relevant information in neuronal networks, for example the presence of the optimal stimulus in the neurons' receptive field. This possibility fits well with the long-suggested role of γ -band fluctuations in synchronizing the activity of neuronal ensembles and binding the descriptions of an object (Eckhorn *et al.*, 1988; Gray & Singer, 1989; Singer, 1993, 1999). It is also in line with recent results suggesting that γ -band activity plays a role in controlling sensory responses, the performance of cortical networks, and selective attention (Jensen *et al.*, 2007; Lakatos *et al.*, 2008; Cardin *et al.*, 2009; Sohal *et al.*, 2009).

Simulated responses of the model neuron – what they reproduce and what they show

Simulated responses of the model neuron to different orientations of moving gratings reproduced well the membrane potential traces, their spectral composition, and other implemented features.

Simulations clearly reveal mutual shunting effects between the low-frequency (stimulus) and the high-frequency fluctuations. Because of the stimulus-induced periodic modulation of the input conductance, shunting effects might be stronger during peaks of slow depolarizations. Furthermore, voltage-dependent mechanisms of neuronal membranes may lead to a sublinear or supralinear summation of synaptic inputs impinging on the neuron (Häusser *et al.*, 2000). These factors disturb the relationship of the membrane potential changes with the underlying conductances, making it non-uniform over the alternating depolarization and hyperpolarization phases of response to the periodic stimulus. Indeed, in the simulations, we had to implement a much stronger modulation of the γ -band conductances by the amplitude of slow depolarization to reproduce the values of correlation coefficients seen in the membrane potential recordings. This indicates that the real difference between the depolarization peaks and hyperpolarization troughs in the strength of γ -range conductance might be even higher

than assessed from the membrane potential traces. An implication of these simulation results is that the γ -power is clearly non-evenly (non-randomly) distributed between slow depolarizations and hyperpolarizations – otherwise, the shunting by the low-frequency conductance changes should have led to a negative correlation, which we never observed in the recordings. This points towards an intrinsic relationship between the γ -band activity and low-frequency depolarizations, and is compatible with the above-mentioned possibility that it is an inherent property of the activity in neuronal networks to be γ -structured.

Comparison of the simulated responses of the model neuron subject to three different classes of input (stimulus alone, unmodulated gamma, and modulated gamma – see Results for details) showed that only the most complete model, with the γ -activity modulated by the phase of slow depolarizations, reproduced faithfully the firing rates and information rates seen in the recorded neuron. In contrast, with both types of input lacking modulated γ -activity, the stimulus alone and the unmodulated gamma, the firing rates and information rates in the model neuron were well below the recorded data. Thus, an increase in the γ -activity as such, without its modulation by the phase of stimulus frequency depolarizations, brings about only a small enhancement of the firing and little improvement in the encoding. Of course, unmodulated γ -activity at the input could still be useful for the detection of weak stimuli, causing an effect similar to stochastic resonance (Anderson *et al.*, 2000a; Volgushev & Eysel, 2000; see Moss *et al.*, 2004 for a review). However, this effect does work in a relatively narrow range of the relationships between the threshold, the amplitude of the high-frequency fluctuations ('noise' in stochastic resonance), and the stimulus strength. Apparently, the values that we measured in neuronal responses to strong sensory stimuli and implemented in the model were outside that range. With the measured ranges of parameters, modulation of the γ -activity by the stimulus frequency membrane depolarization resulted in a substantial increase in the firing rates and improvement in the stimulus encoding.

Limitations of the model

Several limitations of our model are worth mentioning. First, excitatory and inhibitory conductances were simulated as net conductances in the soma. Specific mechanisms of the origin of γ -band fluctuations of the membrane potential caused by the precise temporal organization of excitatory and inhibitory inputs with a contribution of intrinsic membrane properties have been studied in detail elsewhere (Jagadeesh *et al.*, 1992; Jahnsen & Karnup, 1994; Gutfreund *et al.*, 1995; Gray & McCormick, 1996; Hutcheon *et al.*, 1996; Bringuier *et al.*, 1997; Lampl *et al.*, 1999; Azouz & Gray, 2003, 2008; Cunningham *et al.*, 2004; Hasenstaub *et al.*, 2005; Bartos *et al.*, 2007; Sohal *et al.*, 2009). As the origin of γ -band fluctuations was beyond the scope of the present study, we did not implement in the model specific mechanisms of the precise temporal organization of excitatory and inhibitory inputs, or details of the spatial and temporal integration of numerous synaptic inputs impinging on the dendrites. Because of the presence of active ionic conductances and reversal potentials, the spectral composition of the membrane potential fluctuations is not necessarily Gaussian or filtered Gaussian, as implemented in our model. Moreover, it might be possible to adjust the spectral composition of the simulated membrane potential traces to those recorded with a different combination(s) of stochastic processes than the one employed by us. However, Destexhe *et al.* (2001, 2003) demonstrated that filtered Gaussian provides a reasonably good approximation of membrane potential fluctuations, so we opted for this mathematically easily tractable generation of conductances. Furthermore, qualitatively similar dependences of the stimulus

encoding and information rates on the strength and modulation of the γ -band fluctuations were obtained in preliminary simulations for this study, in which modulation of high-frequency fluctuations by the stimulus was implemented by adjusting only excitatory conductance (data not shown). Thus, the main results of the simulations reported here reveal genuine effects of the γ -band fluctuations on stimulus encoding that might be robust to changes in specific mechanisms producing the γ -band fluctuations. Interestingly, a recent study has demonstrated that rapid transient depolarizations preceding action potentials can indeed be produced by either mechanism: increased excitatory conductance, or a combined increase in the excitatory and decrease in the inhibitory conductance (Azouz & Gray, 2008).

Second, for simulations, we used a conductance-based model with Hodgkin–Huxley-type channels. As stimulus encoding in model neurons depends on the properties of the action potential generation mechanism (Fourcaud-Trocmé *et al.*, 2003; Naundorf *et al.*, 2005), we adjusted parameters of the kinetic equations to achieve a better correspondence between the simulated and the recorded action potentials. Although a recent study demonstrated that the Hodgkin–Huxley-type models cannot precisely describe the initiation dynamics of cortical action potentials (Naundorf *et al.*, 2006), there is still no simple and approved model available for an alternative description. For that reason, we decided to use the Hodgkin–Huxley-type model with 'tuned' channel kinetics. Moreover, as rapid dynamics of action potential initiation is beneficial for the encoding of fast signals (Fourcaud-Trocmé *et al.*, 2003; Naundorf *et al.*, 2005, 2006), such as γ -range fluctuations, it may even facilitate the effects of fast membrane potential fluctuations on stimulus encoding reported here.

Finally, we restricted our analysis of encoding to the most simple stimuli, high-contrast moving sinusoidal gratings. We opted for these stimuli for several reasons. Synaptic input to simple cells produced by sinusoidal gratings is well defined and is clearly related to the stimulus. Both the low-frequency component of the membrane potential changes and the power of high-frequency membrane potential fluctuations are clearly modulated at the temporal frequency of the moving grating. These properties of the input can be quantified in a straightforward way and then used as constraints for tuning the model parameters. Furthermore, simple cells encode the temporal frequency of the stimulus in their firing. Thus, for simple neurons subjected to stimulation with sinusoidal gratings, both the input and its encoding in the output signal are well defined, making them an ideal experimental model for studying the influence of input characteristics on stimulus encoding. For linear responses, for example of true simple cells, the results obtained with sinusoidal gratings can be generalized to other stimuli with richer temporal structure. In the presence of nonlinearities, generalization is not possible. However, in that case, the neurons' input produced by visual stimulation *in vivo* and its spectral composition are not defined as clearly as in the case of linear simple cells, hindering direct comparison of the results obtained in experiments and in computer simulations.

Modulated γ -band activity and stimulus encoding

Fast γ -band fluctuations of the membrane potential possess several features that make them especially well suited to subservise synchronization of neuronal activity and/or binding of object representations (Eckhorn *et al.*, 1988; Gray & Singer, 1989; Singer, 1993, 1999). These features include the ability to support reliable spike generation, impose precise temporal windows for synaptic integration, and produce precise temporal patterns of activity (Lampl & Yarom, 1993; Mainen & Sejnowski, 1995; Nowak *et al.*, 1997; Volgushev

et al., 1998, 2003; Salinas & Sejnowski, 2000; Azouz & Gray, 2003, 2008). Moreover, γ -band fluctuations may modify the gain at which membrane depolarizations are translated into spike responses (Volgushev *et al.*, 2002). As the strongest γ -fluctuations are associated with the peaks of slow membrane depolarizations, we have suggested that the modulation of the γ -power by the phase of the low-frequency membrane potential changes might improve stimulus encoding (Volgushev *et al.*, 2003, 2004). This suggestion is in agreement with earlier theoretical results showing that modulation of high-frequency noise intensity is an efficient way to transmit signals through neuronal ensembles (Lindner & Schimansky-Geier, 2001). Here, we show that higher information transmission efficiency can indeed be achieved with modulation of the γ -range fluctuations within the experimentally observed range. Alteration of the strength of the γ -range fluctuations had an even stronger effect on both the firing rate and the information rate than variation of the strength of the low-frequency (stimulus) component of the input. Furthermore, firing of the model neuron exhibited a clear and strong dependence on the degree of modulation of the γ -power by the stimulus. This effect was clearly present in both modifications of the model, either when the modulation influenced the total γ -power by shunting effects of the low-frequency depolarizations, or when the model was compensated for that shunting and the total γ -power remained constant (see Results; Figs 9 and 10). Thus, not just the net depolarization, but also the fine temporal structure of the input, is critical for enhancing spike responses and transmitting information at high rates. In turn, precise temporal organization at the inputs might produce a precisely patterned spike output of the cells, and thus a precise temporal pattern of activity at the inputs to the next-level neurons. Taken together, these properties allow the γ -band activity not only to improve stimulus encoding in every single neuron, but also to facilitate propagation of the encoded information through multiple processing layers of the neuronal network.

Acknowledgements

We are grateful to Tatjana Tchumatchenko for comments on the manuscript. This work was supported by the DFG (SFB 509 TP A5 to MV), the BMBF (grants 01GQ0414 to KO and 01GQ07112 to MV), and start-up funds from the University of Connecticut to MV.

Abbreviations

FFT, fast Fourier transform; SD, standard deviation.

References

- Anderson, J.S., Lampl, I., Gillespie, D.C. & Ferster, D. (2000a) The contribution of noise to contrast invariance of orientation tuning in cat visual cortex. *Science*, **290**, 1968–1972.
- Anderson, J.S., Lampl, I., Reichova, I., Carandini, M. & Ferster, D. (2000b) Stimulus dependence of two-state fluctuations of membrane potential in cat visual cortex. *Nat. Neurosci.*, **3**, 617–621.
- Azouz, R. & Gray, C.M. (1999) Cellular mechanisms contributing to response variability of cortical neurons in vivo. *J. Neurosci.*, **19**, 2209–2223.
- Azouz, R. & Gray, C.M. (2003) Adaptive coincidence detection and dynamic gain control in visual cortical neurons in vivo. *Neuron*, **37**, 513–523.
- Azouz, R. & Gray, C.M. (2008) Stimulus-selective spiking is driven by the relative timing of synchronous excitation and disinhibition in cat striate neurons in vivo. *Eur. J. Neurosci.*, **28**, 1286–1300.
- Bartos, M., Vida, I. & Jonas, P. (2007) Synaptic mechanisms of synchronized gamma oscillations in inhibitory interneuron networks. *Trends in Neurosci.*, **8**, 45–56.
- Bialek, W., Rieke, F., de Ruyter van Steveninck, R.R. & Warland, D. (1991) Reading a neural code. *Science*, **252**, 1854–1857.
- Borst, A. & Theunissen, F.E. (1999) Information theory and neural coding. *Nat. Neurosci.*, **2**, 947–957.
- Bringuier, V., Fregnac, Y., Baranyi, A., Debanne, D. & Shulz, D.E. (1997) Synaptic origin and stimulus dependency of neuronal oscillatory activity in the primary visual cortex of the cat. *J. Physiol. (Lond.)*, **500**, 751–774.
- Carandini, M. & Ferster, D. (2000) Membrane potential and firing rate in cat primary visual cortex. *J. Neurosci.*, **20**, 470–484.
- Cardin, J.A., Carlen, M., Meletis, K., Knoblich, U., Zhang, F., Deisseroth, K., Tsai, L.H. & Moore, C.I. (2009) Driving fast-spiking cells induces gamma rhythm and controls sensory responses. *Nature*, **459**, 663–667.
- Cunningham, M.O., Whittington, M.A., Bibbig, A., Roopun, A., LeBeau, F.E., Vogt, A., Monyer, H., Buhl, E.H. & Traub, R.D. (2004) A role for fast rhythmic bursting neurons in cortical gamma oscillations in vitro. *Proc. Natl Acad. Sci. USA*, **101**, 7152–7157.
- Dean, A.F. & Tolhurst, D.J. (1983) On the distinctness of simple and complex cells in the visual cortex of the cat. *J. Physiol. (Lond.)*, **344**, 305–325.
- Destexhe, A., Rudolph, M., Fellous, J.-M. & Sejnowski, T.J. (2001) Fluctuating synaptic conductances recreate in-vivo like activity in neocortical neurons. *Neuroscience*, **107**, 13–24.
- Destexhe, A., Rudolph, M. & Paré, D. (2003) The high-conductance state of neocortical neurons. *Nat. Rev. Neurosci.*, **4**, 739–751.
- Eckhorn, R., Bauer, R., Jordan, W., Brosch, M., Kruse, W., Munk, M. & Reibcke, H.J. (1988) Coherent oscillations: a mechanism of feature linking in the visual cortex? *Biol. Cybern.*, **60**, 121–130.
- Fourcaud-Trocmé, N., Hansel, D., van Vreeswijk, C. & Brunel, N. (2003) How spike generation mechanisms determine the neuronal response to fluctuating inputs. *J. Neurosci.*, **23**, 11628–11640.
- Fries, P. (2009) Neuronal gamma-band synchronization as a fundamental process in cortical computation. *Annu. Rev. Neurosci.*, **32**, 209–224.
- Fries, P., Nikolic, D. & Singer, W. (2007) The gamma cycle. *Trends Neurosci.*, **30**, 309–316.
- Gabbiani, F. (1996) Coding of time-varying signals in spike trains of linear and half-wave rectifying neurons. *Network*, **7**, 61–85.
- Gray, C.M. & McCormick, D.A. (1996) Chattering cells – superficial pyramidal neurons contributing to the generation of synchronous oscillations in the visual cortex. *Science*, **274**, 109–113.
- Gray, C.M. & Singer, W. (1989) Stimulus-specific neuronal oscillations in orientation columns of cat visual cortex. *Proc. Natl Acad. Sci. USA*, **86**, 1698–1702.
- Gutfreund, Y., Yarom, Y. & Segev, I. (1995) Subthreshold oscillations and resonant frequency in guinea-pig cortical neurons: physiology and modeling. *J. Physiol.*, **483**, 621–640.
- Hasenstaub, A., Shu, Y., Haider, B., Kraushaar, U., Duque, A. & McCormick, D.A. (2005) Inhibitory postsynaptic potentials carry synchronized frequency information in active cortical networks. *Neuron*, **47**, 423–435.
- Häusser, M., Spruston, N. & Stuart, G.J. (2000) Diversity and dynamics of dendritic signaling. *Science*, **290**, 739–744.
- Hutcheon, B., Miura, R.M. & Puil, E. (1996) Subthreshold membrane resonance in neocortical neurons. *J. Neurophysiol.*, **76**, 683–697.
- Jagadeesh, B., Gray, C.M. & Ferster, D. (1992) Visually evoked oscillations of membrane potential in cells of cat visual cortex. *Science*, **257**, 552–554.
- Jahnsen, H. & Kamup, S. (1994) A spectral analysis of the integration of artificial synaptic potentials in mammalian central neurons. *Brain Res.*, **666**, 9–20.
- Jensen, O., Kaiser, J. & Lachaux, J.P. (2007) Human gamma-frequency oscillations associated with attention and memory. *Trends Neurosci.*, **30**, 317–324.
- Lakatos, P., Karmos, G., Mehta, A.D., Ulbert, I. & Schroeder, C.E. (2008) Entrainment of neuronal oscillations as a mechanism of attentional selection. *Science*, **320**, 110–113.
- Lampl, I. & Yarom, Y. (1993) Subthreshold oscillations of the membrane potential: a functional synchronizing and timing device. *J. Neurophysiol.*, **70**, 2181–2186.
- Lampl, I., Reichova, I. & Ferster, D. (1999) Synchronous membrane potential fluctuations in neurons of the cat visual cortex. *Neuron*, **22**, 361–374.
- Lindner, B. & Schimansky-Geier, L. (2001) Transmission of noise coded versus additive signals through a neuronal ensemble. *Phys. Rev. Lett.*, **86**, 2934–2937.
- Mainen, Z.F. & Sejnowski, T.J. (1995) Reliability of spike timing in neocortical neurons. *Science*, **268**, 1503–1506.
- Moss, F., Ward, L.M. & Sannita, W.G. (2004) Stochastic resonance and sensory information processing. A tutorial and review of applications. *Clin. Neurophysiol.*, **115**, 267–281.

Mukovski, M., Chauvette, S., Timofeev, I. & Volgushev, M. (2006) Detection of active and silent states in neocortical neurons from the field potential signal during slow wave sleep. *Cereb. Cortex*, **17**, 400–414.

Naundorf, B., Geisel, T. & Wolf, F. (2005) Action potential onset dynamics and the response speed of neuronal populations. *J. Comput. Neurosci.*, **18**, 297–309.

Naundorf, B., Wolf, F. & Volgushev, M. (2006) Unique features of action potential initiation in cortical neurons. *Nature*, **440**, 1060–1063.

Nowak, L.G., Sanchez-Vives, M.V. & McCormick, D.A. (1997) Influence of low and high frequency inputs on spike timing in visual cortical neurons. *Cereb. Cortex*, **7**, 487–501.

Rieke, F., Warland, D., de Ruyter van Steveninck, R.R. & Bialek, W. (1997) *Spikes: Exploring the Neural Code*. MIT Press, Cambridge.

Salinas, E. & Sejnowski, T.J. (2000) Impact of correlated synaptic input on output firing rate and variability in simple neuronal models. *J. Neurosci.*, **20**, 6193–6209.

Singer, W. (1993) Synchronization of cortical activity and its putative role in information processing and learning. *Annu. Rev. Psychol.*, **55**, 349–374.

Singer, W. (1999) Neuronal synchrony: a versatile code for the definition of relations? *Neuron*, **24**, 49–65.

Skottun, B.C., Valois, R.L., Grosz, D.H., Moshon, J.A., Albrecht, D.G. & Bonds, A.B. (1991) Classifying simple and complex cells on the basis of response modulation. *Vision Res.*, **31**, 1079–1086.

Sohal, V.S., Zhang, F., Yizhar, O. & Deisseroth, K. (2009) Parvalbumin neurons and gamma rhythms enhance cortical circuit performance. *Nature*, **459**, 698–702.

Steriade, M., Contreras, D., Amzica, F. & Timofeev, I. (1996) Synchronization of fast (30–40 Hz) spontaneous oscillations in intrathalamic and thalamo-cortical networks. *J. Neurosci.*, **16**, 2788–2808.

Volgushev, M. & Eysel, U.T. (2000) Noise makes sense in neuronal computing. *Science*, **290**, 1908–1909.

Volgushev, M., Chistiakova, M. & Singer, W. (1998) Modification of discharge patterns of neo-cortical neurons by induced oscillations of the membrane potential. *Neuroscience*, **83**, 15–25.

Volgushev, M., Pernberg, J. & Eysel, U.T. (2000) Comparison of the selectivity of postsynaptic potentials and spike responses in cat visual cortex. *Eur. J. Neurosci.*, **12**, 257–263.

Volgushev, M., Pernberg, J. & Eysel, U.T. (2002) A novel mechanism of response selectivity of neurons in cat visual cortex. *J. Physiol. (Lond.)*, **540**, 307–320.

Volgushev, M., Pernberg, J. & Eysel, U.T. (2003) γ -Frequency fluctuations of the membrane potential and response selectivity in visual cortical neurons. *Eur. J. Neurosci.*, **17**, 1768–1776.

Volgushev, M., Pernberg, J. & Eysel, U.T. (2004) Response selectivity and gamma-frequency fluctuations of the membrane potential in visual cortical neurons. *Neurocomputing*, **58–60**, 957–963.

Wang, X.J. & Buzsaki, G. (1996) Gamma oscillation by synaptic inhibition in a hippocampal interneuronal network model. *J. Neurosci.*, **16**, 6402–6413.

Appendix

The Hodgkin–Huxley neuron

Here, we describe the model equations for the conductance-based model in detail. The membrane potential V of the model neuron changes in time according to the following differential equation:

$$C_m \frac{dV}{dt} = -I_L - I_{Na} - I_K - I_M - I_{syn}, \quad (A1)$$

where $C_m = 1 \mu\text{F}/\text{cm}^2$ is the membrane capacitance, $I_L = g_L (V - E_L)$ is the leak current, $g_L = 0.05 \text{ mS}/\text{cm}^2$ is the leak conductance, and $E_L = -75 \text{ mV}$ is the resting membrane potential. I_{Na} and I_K are the voltage-gated sodium and potassium currents that mediate action potential generation, and I_M is a non-inactivating potassium current mediating spike frequency adaptation. The kinetic equations for I_{Na} , I_K and I_M were taken from a single-compartment model of an interneuron (Wang & Buzsaki, 1996), and adapted such that the shape of the action potential is close to that of the recorded action potential. Specifically, to bring the initiation dynamics of action potentials in the model closer to the fast spike onset dynamics observed in neocortical neurons (Naundorf *et al.*, 2006), we set the kinetics of sodium channels 10 times faster, and the width of their activation curve two times narrower, than in the original model. All simulations in this article were performed with a time step of $dt = 0.05 \text{ ms}$.

Voltage-dependent sodium current

$$\begin{aligned} I_{Na} &= \bar{g}_{Na} m_\infty^3 h (V - E_{Na}) \\ m_\infty &= \frac{\alpha_m(V)}{\alpha_m(V) + \beta_m(V)} \\ \frac{dh}{dt} &= \alpha_h(V) (1 - h) - \beta_h(V) h \\ \alpha_m(V) &= \frac{-0.25 (V + 41)}{\exp(-0.25 [V + 41]) - 1} \\ \beta_m(V) &= 4 \exp(-[V + 60]/18) \\ \alpha_h(V) &= 0.07 \exp(-[V + 58]/20) \\ \beta_h(V) &= \frac{1}{1 - \exp(-0.1 [V + 28])} \end{aligned} \quad (A2)$$

Model parameters – $g_{Na} = 25 \text{ mS}/\text{cm}^2$ and $E_{Na} = 55 \text{ mV}$.

Delayed rectifier potassium current

$$\begin{aligned} I_K &= \bar{g}_K n^4 (V - E_K) \\ \frac{dn}{dt} &= \alpha_n(V) (1 - n) - \beta_n(V) n \\ \alpha_n(V) &= \frac{-0.01 (V + 54)}{\exp(-0.3 [V + 54]) - 1} \\ \beta_n(V) &= 0.15 \exp(-[V + 28]/30). \end{aligned} \quad (A3)$$

Model parameters – $g_K = 4 \text{ mS}/\text{cm}^2$ and $E_K = -90 \text{ mV}$.

Non-inactivating potassium current

$$\begin{aligned} I_M &= \bar{g}_M p (V - E_K) \\ \tau_p \frac{dp}{dt} &= p_\infty(V) - p \\ \tau_p(V) &= \frac{1000}{3.3 (\exp([V + 35]/40) + \exp(-[V + 35]/20)) T_{adj}} \\ p_\infty(V) &= \frac{1}{1 + \exp(-[V + 35]/10)}. \end{aligned} \quad (A4)$$

Model parameters – $g_M = 1.2 \text{ mS}/\text{cm}^2$, $T_{adj} = 4.656$, and $E_K = -90 \text{ mV}$.